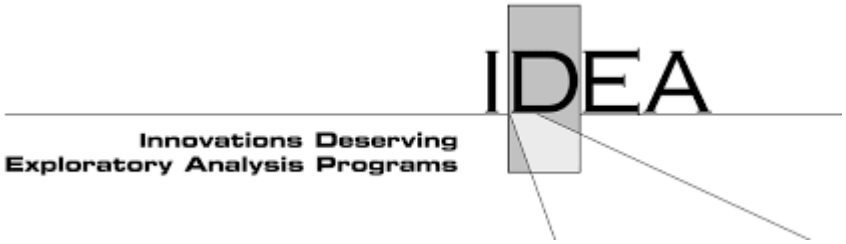

Rail Safety IDEA Program

Dynamic Impact Factors on Existing Long Span Truss Railroad Bridges

Final Report for
Rail Safety IDEA Project 25

Prepared by:
Ramesh B. Malla, Ph.D.
David Jacobs, P.E.
Suvash Dhakal
Surendra Baniya

University of Connecticut
.

February 2017

TRB TRANSPORTATION RESEARCH BOARD
The National Academies of
SCIENCES • ENGINEERING • MEDICINE

Innovations Deserving Exploratory Analysis (IDEA) Programs Managed by the Transportation Research Board

This IDEA project was funded by the Rail Safety IDEA Program.

The TRB currently manages the following three IDEA programs:

• NCHRP IDEA Program, which focuses on advances in the design, construction, and maintenance of highway systems, is funded by American Association of State Highway and Transportation Officials (AASHTO) as part of the National Cooperative Highway Research Program (NCHRP).

• The Rail Safety IDEA Program currently focuses on innovative approaches for improving railroad safety or performance. The program is currently funded by the Federal Railroad Administration (FRA). The program was previously jointly funded by the Federal Motor Carrier Safety Administration (FMCSA) and the FRA.

• The Transit IDEA Program, which supports development and testing of innovative concepts and methods for advancing transit practice, is funded by the Federal Transit Administration (FTA) as part of the Transit Cooperative Research Program (TCRP).

Management of the three IDEA programs is coordinated to promote the development and testing of innovative concepts, methods, and technologies.

For information on the IDEA programs, check the IDEA website (www.trb.org/idea). For questions, contact the IDEA programs office by telephone at (202) 334-3310.

IDEA Programs

Transportation Research Board

500 Fifth Street, NW

Washington, DC 20001

Dynamic Impact Factors on Existing Long Span Truss Railroad Bridges

Final Report

IDEA Project RS – 25

Prepared for the
Rail Safety IDEA Program
Transportation Research Board
National Research Council
Washington, D.C. 20001

Prepared by

Principal Investigator
Ramesh B. Malla, Ph.D., F. ASCE, Professor

Graduate Assistants
David Jacobs, P.E.; Suvash Dhakal; and Surendra Baniya

Structural Engineering and Applied Mechanics
Department of Civil & Environmental Engineering
University of Connecticut
Storrs, CT 06269-3037

RAIL SAFETY IDEA PROGRAM COMMITTEE

CHAIR
CONRAD J. RUPPERT, JR
University of Illinois at Urbana-Champaign

MEMBERS
TOM BARTLETT
Union Pacific Railroad
MELVIN CLARK
Capital Metropolitan Authority
MICHAEL FRANKE
National Railroad Passenger Corporation (Amtrak)
PETER FRENCH
Association of American Railroads(Ret.)
BRAD KERCHOF
Norfolk Southern Railway
MARTITA MULLEN
Canadian National Railway
STEPHEN M. POPKIN
Volpe National Transportation Systems Center

FRA LIAISON
TAREK OMAR
Federal Railroad Administration

NTSB LIAISON
ROBERT HALL
National Transportation Safety Board

TRB LIAISON
SCOTT BABCOCK
Transportation Research Board

IDEA PROGRAMS STAFF
STEPHEN R. GODWIN, *Director for Studies and Special Programs*
JON M. WILLIAMS, *Program Director, IDEA and Synthesis Studies*
JO ALLEN GAUSE, *Senior Program Officer*
DEMISHA WILLIAMS, *Senior Program Assistant*

EXPERT REVIEW PANEL
SAFETY IDEA PROJECT 25
RONALD BOTTACARI, *MTA Metro–North Railroad Company (retired)*
RICHARD BRAY, *H.W. Lochner, Inc.*
STEPHEN DICK, *Transportation Technology Center, Inc*
MICHAEL FRANKE, *Amtrak*

ACKNOWLEDGMENTS

The principal investigator of the project would like to acknowledge and thank the following individuals and organizations whose support (financial, material, and/or in-kind) assisted in this research and significantly contributed to the success of the project:

- Graduate assistants involved in this project:
  - Surendra Baniya, M.S. student
  - Suvash Dhakal, Ph.D. student
  - David Jacobs, Ph.D. student

- The U.S. Department of Transportation (DOT) Federal Railroad Administration (FRA) for project funding. This project is part of the Rail Safety IDEA Program managed by Transportation Research Board (TRB). Special thanks to Ms. Jo Allen Gause, Senior Program Officer at TRB, the manager for this research project for all her unfailing support, constant encouragement, advice, and patience. Thanks are also due to Mr. Charles Taylor, Program Manager at TRB for his support in the initial phase of this project.

- The Connecticut Department of Transportation, Newington, Connecticut, for their support making the Devon railroad bridge available for testing and other in-kind contribution.

- Bentley Systems, Inc., Exton, PA/Watertown, CT for their cost-share financial support (Contact: Dr. Zheng Wu, Bentley Fellow and Director of Applied Research).

- MTA Metro–North Railroad Company (Mr. Joseph J. Giulietti, President; Mr. Glen E. Hayden, Vice President—Engineering; Mr. Rajendra Kasbawala; Mr. Dan McCarthy; and others) for making test trains available to the research team, facilitating access to Devon Bridge, and other support essential to the successful completion of this research project.

- National Railroad Passenger Corporation (Amtrak) (Mr. David Staplin and Mr. Mike Trosino) for making their Acela test trains available to the research team.

- The following additional companies whose contributions were necessary and essential to the research effort:
  - STRAAM, Inc., New York, NY, for their support in field tests (Contacts: Dr. Alan Jeary and Mr. Thomas Winant).
  - TRANS-TEK, Inc., Ellington, CT, for providing field test instruments.
  - BDI, Inc., Boulder, CO, for providing supplemental testing equipment.

- The following members of the project's Expert Panel for their time and attention providing many valuable comments during the course of this project:
  - Ronald M. Bottacari, P.E., MTA Metro–North Railroad Company (retired)
  - Richard A. Bray, P.E., H.W. Lochner, Inc., East Hartford, CT
  - Stephen M. Dick, Ph.D., P.E., Transportation Technology Center, Inc., Pueblo, CO
  - Michael W. Franke, Amtrak, Chicago, IL

- The following University of Connecticut Civil & Environmental Engineering Department graduate students who assisted significantly in the field testing:
  - Dominic Kruszewski, M.S. student
  - Luis Villa, Ph.D. student

- Last, but not least, the University of Connecticut, its Department of Civil and Environmental Engineering, and Connecticut Transportation Institute (CTI) for cost share, in-kind support, laboratory facilities, and project administration help.

TABLE OF CONTENTS

LIST OF FIGURES

LIST OF TABLES

1. EXECUTIVE SUMMARY

The main goal of the research was to study and investigate the dynamic live load impact on older long-span steel truss railroad bridges, with special consideration for the effects of the higher train speeds. The study and investigation were based on analytical/computational (finite element) modeling/analysis and field testing on an existing bridge. There were three specific objectives of this study. The first objective was to develop an accurate finite element (FE) model of an existing long-span truss bridge selected for this study. The second objective was field testing of the subject bridge with actual trains of varying consists, axle loads, axle spacings, and traveling speeds. The third objective was to compare the results from the analytical/computational model with the field test results, verify the model, and develop/recommend a procedure to help understanding the effects of train speeds on dynamic impact factors for the bridge, especially at train speeds higher than the current allowable operating speed limit. The stated objectives of the project were fully achieved with work performed in two stages, Stage 1 and 2. The main focus in Stage 1 was the development of the FE modeling of the test bridge along with initial field testing and comparison of the results. Stage 2 focused on further detail field testing of the bridge with trains traveling at varying speeds, comparison of results and refinement of the FE model, and investigation on resonance speed of the trains for the bridge.

The long-span open deck truss bridge used for this study was the Connecticut Department of Transportation's Devon railroad bridge over the Housatonic River, between Milford and Stratford. Specifically, all testing was performed on span 7 (next to the eastern abutment) of the seven span north bridge. The span is a 66.32 m (217ft -7 in.) 2-track, open deck, pin connected through steel truss, opened in 1907.

For the analytical/computation study, a comprehensive FE model of the Devon Bridge was created using the STAAD.Pro V8*i* structural software code. Beam and truss elements were utilized in preparing the FE model, with the boundary conditions closely representative to the actual truss, including the floor (railway track) and bracing systems. A total of 4,371 nodes and 5,316 elements comprised the model. Modal parameters (natural frequencies and mode shapes) and responses (displacement, stresses) of the bridge were obtained under static and dynamic train loading.

A series of tests were conducted on 12 separate occasions, over a 15-month period, with four types of trains: Metro–North M8 commuter cars, Metro–North Waterbury Branch trains (diesel engine with standard coaches), Amtrak Regional trains (electric locomotive with standard coaches), and Amtrak Acela trains (electric locomotive at each end, with Acela coaches in between). The bridge responses under the trains travelling at various speeds, including 8.0, 16.1, 32.2, 48.8, and 64.4 km/h (5, 10, 20, 30, and 40 mph, the current speed limit over the bridge), were measured using strategically placed sensors [accelerometers, strain gages, and linear variable differential/displacement transducers, (LVDTs)]. The accelerometers were used to measure vibration accelerations in three directions, longitudinal (along the length of the bridge), vertical, and lateral directions. LVDTs were used to measure vertical displacements of the bottom of the bridge. Strain gages were used to measure strains in diagonals, bottom chord, and vertical members of the truss and the rails. The field-collected accelerometer data were analyzed to obtain the natural frequencies and the mode shapes of the bridge. Several delays due to weather and un-availability of test train equipment and crews were encountered during the field test portion of the project, resulting in this phase of the work taking longer to complete than initially planned.

The results from the field tests were compared with the values obtained from the FE model and analysis. The FE model was then updated. Good correlation was achieved between the bridge responses obtained from the field test data and the FE model, thus confirming the validity of the analytical/computational model for static and dynamics loading. The updated model was then used to obtain the response of the bridge under different types of trains moving at speeds higher than the currently allowable maximum speed of 64.4 km/h (40 mph). The resonance speeds in vertical and lateral directions for Amtrak Acela, Amtrak Regional, and Metro–North M8 trains on the Devon Bridge were determined and identified using the finite element and analytical relations. From the field obtained data, it was observed that there was negligible difference in the magnitudes of vertical displacement of the bridge under trains moving at different speeds including 8.0, 16.1, 32.2, 48.8, and 64.4 km/h (5, 10, 20, 30, and 40 mph) within the maximum allowable speed limit of 64.4 km/h (40 mph). However, from the results obtained using the updated FE model of the bridge, it was found that there was an increase in displacement of a node of the bridge at certain speeds of the trains that are relatively close to the resonance frequencies of the bridge.

The knowledge gained and results obtained from this research study should contribute to (a) improving railroad safety, (b) reducing the costs of upgrading existing railroad bridges to accommodate higher speed trains, (c) more accurately predicting remaining life, (d) improving rating of the structures, and (e) increasing structure reliability. Although this study has highlighted the possible effects of speed on the dynamic impact factor on an existing long-span truss railroad

bridge, there are several areas in which further research studies are needed including development of the actual relationship between speed and impact factor on the bridge, incorporation of the interaction between the moving vehicle and the bridge dynamics in the analytical modeling, investigation of effects of the lateral force caused by passing of the train, determination of moving dynamic load time history over the railroad bridge from limited field test data, determination of resonance and cancellation speeds of a moving train considering the bridge as an actual truss railroad bridge, rocking effects on a truss bridge; and conducting field testing of the bridge at higher train speeds for validating FE/analytical models.

2. IDEA PRODUCT

The main goal of the research was to study and investigate the dynamic/live load impact on older long-span, open deck steel truss railroad bridges and to understand the effects of higher speed trains. The methodology was based on analytical/ finite element analysis and field testing on an existing bridge. The first specific objective of this study was to develop an accurate finite element model (FEM) of the selected existing older long-span truss bridge. The second was the field testing of the subject bridge with trains of varying consists, axle loads, axle spacing, and speeds traversing over the bridge. The third specific objective was to compare the results from the analytical/computational model with the field test results, verify the model, and develop/recommend a procedure to help understand the effects of train speeds on the dynamic impact factors for the bridge, especially for train speeds higher than the current allowable operating speed. The work was performed in two stages. In Stage 1, a detail FEM was built and analyzed, followed by some initial field testing and comparison of the results. The main focus in Stage 1 was the development of the finite element modeling of the test bridge, initial field testing, and comparison of the results. Stage 2 included a more detail field testing of the bridge with trains traveling at varying speeds, comparison of results and refinement of the FEM, and investigation on resonance speed of the trains for the bridge.

A comprehensive FEM of one of the seven spans of length 66.32 m (217 ft 7 in.) of the 109-year-old, 325.2 m (1,066 ft 10 in.) long, open deck, steel through-truss Devon railroad bridge over the Housatonic River, between Milford and Stratford, Connecticut, was developed using the STAAD.Pro V8*i* structural finite element software code (Bentley 2012). Static, modal, and dynamic analyses of the bridge under moving trains were performed to obtain bridge responses (displacement, stresses, frequencies, and mode shapes). Several field tests were conducted on the bridge span under four types of trains: Amtrak Acela, Amtrak Regional, Metro–North M8 trains, and Waterbury Branch trains with diesel engine and standard coaches. Using five types of sensors [foil strain gages (Omega 2016), clamp-on strain gages (BDI 2012), uniaxial accelerometers (BDI 2013), tri-axial accelerometer (Trimble 2015), and linear variable differential transducers, LVDTs (TransTek 2015)] strategically placed on the bridge; accelerations, strains, and displacements were recorded. The field test results were compared with those obtained from the FEM, which was then updated. A strong correlation was achieved, thus confirming the validity of the analytical/computational model. The readjusted model was then used to obtain the resonance train speeds and response of the bridge under different types of trains moving at speeds higher than the currently allowable maximum speed, including at some of the resonance speeds. This information will be useful in understanding the effect of train speeds on the impact factors on the long-span, truss railroad bridges; design of new open deck bridges; and rating of existing bridges. This is particularly useful in situations where existing rights-of-way are being upgraded as new high speed corridors.

3. CONCEPT AND INNOVATION

This research project dealt with the study of static and dynamic response of an open deck, long-span, through-truss railroad bridge, typical of the type of structures designed and built by railroad companies in the United States in the early part of the twentieth century. Many of these bridges are still in service today, and are likely to remain in service for many more years. This research was specifically conducted on a long-span, older, steel truss railroad bridge on the Northeast Corridor that will likely eventually be used to carry the higher speed trains (NAR 2016). Equally important, the bridge used for testing is typical of many existing railroad bridge structures across the United States that will also be used in the future for higher speed trains. On the NEC alone, 45 of the 64 truss bridges are near or exceeding 100 years old. This more specific testing is therefore beneficial for a large number of existing older steel trusses that have been designated for upgrading to accommodate higher speed passenger service (NAR 2016).

In order to understand the live load impact caused by moving trains on the response of the bridge, an FEM of the bridge was developed and analyzed, with speeds varying from 8.0 km/h (5 mph) to the maximum allowable speed on the Devon Bridge of 64.4 km/h (40 mph). The field test results were used to update and validate the FEM so as to obtain strong correlation between the field test and FEM results. With the help of the updated FEM, the response of the bridge was projected for vehicle speeds greater than the currently permissible speed of 64.4 km/h (40 mph).

Among innovations of this research effort are the following: (1) A primary research tool was the use of a continually refined FEM of the bridge in conjunction with data of bridge response obtained from field testing. (2) Extensive analytical analysis was performed regarding vehicle speed and its relationship to vertical and horizontal resonance effects. This area is discussed in detail in the report. (3) Examination of the problem of uneven wear at eyebar holes and connection pins resulting in excessive vibration of some eyebars, and uneven distribution of load in eyebar sets, used in the truss bottom chords and diagonals. Better knowledge of long-span truss bridge response from this study should help bridge engineers better understand how higher speed trains will affect fatigue and life cycle of this type of railroad bridge, resulting ultimately in more efficient, durable, and economic designs of new bridges, and more accurate ratings of existing bridges. This is particularly useful in situations where existing rights-of-way are being upgraded as new high speed corridors, and utilizing to a large extent, existing older structures.

4. INVESTIGATION

For effective, environmentally friendly, economical, and congestion-free transportation in the future, the Federal Railroad Administration (FRA) of the U.S. Department of Transportation (U.S.DOT) is enhancing the railway infrastructure in the nation. Upgrading the railroad infrastructure will also help reduce the traffic congestion on the highways. It has been established by U.S.DOT/FRA that Amtrak's Northeast Corridor (NEC) between Washington, D.C. and Boston, Massachusetts, is one of the highest priority routes in the country chosen for upgrade to high speed rail (Amtrak 2016). It is well-known that open deck trusses are an extremely common railroad bridge design nationwide, especially for spans greater than roughly 45.72 m (150 ft.), as called for in the American Railway Engineering and Maintenance-of-Way Association (AREMA) Manual for Railway Engineering (AREMA 2016). There are 64 individual major open deck truss spans in 11 bridges on Amtrak's Northeast Corridor alone, and nationwide there are a significant number of open deck old truss railroad bridges. The overwhelming majority of these, especially in NEC, are close to or more than 100 years old. The structural integrity and performance of these older existing bridges under future high speed trains are not known and need to be studied. This research study dealt with understanding the dynamic response and impact caused by high speed trains on existing open deck steel truss bridges. The methodology will be based on analytical/computation and field testing of a selected long-span truss bridge in Connecticut.

4.1 IMPACT FACTOR CONCEPT

Dynamic loads coming from moving trains on railroad bridges produce greater stresses in members than those produced by their static counterpart. The dynamic magnification factor (DMF) on a bridge can be defined as the amplification applied to the static response of the structure caused by a force if the same force is now applied in sudden or dynamic fashion, or the ratio of maximum dynamic to maximum static response (e.g., displacement, stress, and stress) being considered (Clough and Penzien 1995). That is,

$$DMF = \frac{\delta_{dyn}}{\delta_{sta}} \quad \text{..... (1)}$$

where δ_{dyn} and δ_{sta} are respectively the maximum dynamic and static responses of the bridge at the same location.

The dynamic impact factor (or simply impact) on a bridge structure can be defined in general as the difference in maximum dynamic response and static response divided by the static response of the structure under a loading; that is,

$$Impact = \frac{\delta_{dyn}-\delta_{sta}}{\delta_{sta}} = \frac{\delta_{dyn}}{\delta_{sta}} - \frac{\delta_{sta}}{\delta_{sta}} = DMF - 1 \quad \text{..... (2)}$$

As can be seen from above, the dynamic impact factor is DMF minus one. Impact factors calculated based on different responses (strain, stress, deflections, force, moment, acceleration, etc.) are not the same. Several studies have found that the impact factor based on deflection is greater than those based on other responses such as strain or acceleration (Yang et al. 1995; McLean and Marsh 1998; Hamidi and Marsh 2010). Therefore, it seems more reasonable to choose the deflection as a controlling parameter (response) for impact factor determination for high speed railroad bridges.

In practice for railroad bridge design, the impact factor is usually used as a fraction or percentage of the live load (AREMA 2016). In design of new and rating of existing railroad bridges in North America, stress (axial, bending, and shear) are normally used. There are many factors/parameters that affect the dynamic behavior of steel railroad bridges; hence, the impact factor for design. Some of them include (Unsworth 2010): (i) span length, (ii) vehicle speed, (iii) dynamic characteristics of the vehicle (mass, suspension system, etc.), (iv) dynamic characteristics of the bridge (mass, stiffness, natural frequencies), (v) track irregularities (joints, tie condition, geometry), (vi) right-of-way anomalies at bridge approach (head blocks, track modulus), (vii) bridge supports (alignment and elevation), (viii) deck type (open, ballasted, direct fixation), (ix) wheel irregularities (flat spots, circular trueness), (x) train characteristics (consist, axle spacing, acceleration, breaking), and (xi) probability of attaining maximum dynamic effect simultaneously with maximum applied load.

This study deals with open deck type bridges (viii) and specifically includes the effects of speed (ii) and vehicle type/axle spacing (x). Among the major bridge impact studies conducted over the last several decades have been those by AREA (1968), BDI (2001), and Uppal et al. (2003).

Research into the phenomenon of impact factor from live load on railroad bridges has been ongoing almost since the beginning of the use of railroads as a form of commercial transportation. The earliest known published work in this area was conducted in Germany in 1848 and in Great Britain in 1849 (Timoshenko 1953). This research has been conducted in many countries around the world; however, there are differences in the specific focus of the various studies. Some studies have looked at the effects of high speed passenger trains, some of heavy axle load freight cars, some on just ballasted decks, and some on open decks, while other studies have concentrated of relating vehicle speed to impact. Many research studies can be found on this general subject matter of railroad bridge impact factor. However, this current study is unique in several respects. First, the test vehicles used were exclusively passenger trains, since a primary focus is to forecast impact with these trains, rather than freight trains, operating at higher speeds. Second, the test structure used was a 110-year-old bridge that will likely be utilized for these higher speed trains. And third, this study utilized a FEM, calibrated specifically to the responses recorded from field tests on the test bridge.

4.2 RAILROAD BRIDGE IMPACT FACTORS

The treatment of impact factors in the design of railroad bridges varies around the world, based on the specifications used in that country or area. In North America, railroad bridge design is based on the AREMA Manual (AREMA 2016). The Commentary section of AREMA Manual states that the current impact formulas are based on investigations and tests of railroad bridges in service (AREMA 2016).

There are many resources that describe the numerous investigations and tests conducted over the last century and a half regarding railroad bridge impact in the United States (see, for example, AREMA 1905, 1910; AREMA—Committee 30 1911; Hunley 1935; AREA Committee 30 1949; AAR 1968; Dhar et al. 1978; Chu et al. 1979; McKeel and Miller 2006). These resources are useful in tracing the evolution of the impacts requirements for North American railroad bridges over that time span.

By 1948, when much more accurate measuring devices were available to researchers, the American Railway Engineering Association (AREA) adopted the basic vertical effect formulas currently in use in North America (Ruble 1955). The dynamic amplification effect from moving trains is incorporated in the live load design requirement by AREMA (2016) and is given as a percentage increase in statically applied Cooper E-loading. The impact percentage of live load to be applied to static live load has two components: vertical effect and rocking effect. The vertical effect formulas are as shown in Eqs. (3) and (4) below:

$$\text{For L less than 80 feet:} \quad 40 - (3L^2 / 1600) \tag{3}$$

$$\text{For L 80 feet or more:} \quad 16 + (600 / (L\text{-}30)) \tag{4}$$

where L = length in feet, center-to-center of supports for stringers, transverse floor beams without stringers, longitudinal girders, and trusses (main members), or L = length, in feet, of the longer adjacent supported stringers, longitudinal beam, girder or truss for impact in floor beams, floor beam hangers, sub-diagonals of trusses, transverse girders, supports for longitudinal, and transverse girders and viaduct columns.

The rocking effect is called for as a "vertical force couple, each being 20% of the wheel load without impact, acting downward on one rail and upward on the other. The couple shall be applied on each track in the direction that will produce the greatest force in the member under consideration." This requirement was adopted by AREA in 1967. The Cooper E-loading is a theoretical live load configuration, with various axle load and spacings. The "80" refers to the heaviest axle load in the configuration, 80 kips (355.9 kN). These formulas (Eqs. 3 and 4) were derived empirically from data obtained from field tests conducted by the Association of American Railroads (AAR) in 1965 (AAR 1968a, 1968b). It should be also mentioned that AREMA (2016) specifies another separate formula $I = 15 + 4000/(L+25)$ for computing the impact vertical effect for truss spans carrying steam locomotives with hammer blow. However, bridges no longer need to sustain the more adverse effects of steam engine hammer blow as modern trains do not use such engines.

4.3 SPEED EFFECTS ON DYNAMIC IMPACT FACTOR

Since the 1930s, greater effort has been given by AREA and AREMA to specifically relate train speed to impact. AREA Committee 30 (1949) concluded that "the magnitude of the roll effect was approximately the same for all speeds. Consequently, it was decided to apply a reduction of impact only to the direct vertical effect." That same report went on to say that "reduction in impact should occur at 64.4 km/h (40 mph) or less." Field test data obtained by AAR in 1965 on truss railroad bridges with a test train running at various speeds showed an increase in impact with an increase in speed, and was most evident in the hangers (AAR 1968a). Similarly, data from the second set of field tests by AAR in 1966 showed an increase in impact with speed in the stringers, floor beams, and hangers (AAR 1968b).

In later years, more studies were done to determine the train speed effects in the response and impact factor of railroad bridges utilizing the analytical and numerical methods. For example, Dhar et al. (1978) and Chu et al. (1979) utilized lumped mass and more refined multi-degree-of-freedom system analytical models, respectively, to study the dynamic response of railroad bridges. From a set of parametric studies they were able to draw several conclusions showing the influence of train speeds on the bridge response and the impact factor. However, of significance to note here is that with the constant refinement of the design impact formulas through additional tests over time, all still relates impact to span length alone, and do not include train speed as a parameter.

AREA, and later AREMA, does recognize a relationship between train speed and impact in the formula for *rating of existing bridge*s. AREMA (2016) allows a reduction in the vertical effect of the impact factor equation for speeds below 96.6 km/h (60 mph) by a multiplication factor given by

$$[1 - \frac{0.8}{2500} (60 - S)^2] \text{ or } 0.2, \text{ whichever is greater, where } S = \text{speed in mph} \quad (5)$$

Reduction in impact is not allowed for rocking effect. The above reduction can be significant on its effect of a structure's rating. For example, a 25 ft. (7.62 m) stringer will have a live load impact factor of 38.8% of static load as given by Eq. (4). If the speeds are 48.8, 32.2, or 16.1 km/h (30, 20, or 10 mph), the values of impact (% of static load) as given by relation (Eq. 5) become approximately 27.6, 18.9, and 7.8, respectively. This in turn means the increase in the rating by 8.8, 16.7, and 28.8%, respectively (Conway 2001).

Research into railroad bridge impact factors has been also conducted in many countries around the world outside of the United States. For example, significant research on this subject has been conducted in Poland by Przemyslaw et al. (2011); Portugal by Rodrigues (2002); China by Zhai et al. (2001); Canada by Pietraszek and Oommen (1991); England by Gu et al. (2008); Spain by Goicolea and Gabaldon (2008) and Goicolea et al. (2008); in the Czech Republic by Fryba (2001); in Australia by Prasad (2009); in Japan by Satoh (1966); and in South Korea by Yoon et al. (2013). In recent years, many studies have dealt with effect of train speed on bridge impact factors, including Hamidi and Danshjoo (2010) and Yoon et al. (2013). However, they deal with mostly girder, not truss, bridges and utilize a simpler beam model for the bridge.

In spite of various research studies and investigations, as of now a significant gap still exists in that the AREMA design specification criterion does not take into account the effects of train speed and the resonance phenomenon due to the periodic nature of the moving train loading on the dynamic response of the bridge. The riding comfort of the passengers and the longevity of the structure can be increased if the critical speed corresponding to the resonant condition can be avoided. This study attempts to better understand the effect of speed on impact factor for railroad bridges.

Presented below is an overview of the analytical formulation of the response of a bridge under a moving load on the bridge using a FEM of the bridge, followed by an examination of data collected from field tests on the bridge. This is followed by a comparison and analysis of the analytic results with the field collected data.

4.4 CONCEPT OF DYNAMIC MAGNIFICATION FACTOR, MOVING LOAD, AND RESONANCE

4.4.1 Dynamic Magnification Factor

Consider a single degree of freedom (SDOF) system with a mass (m) supported by a weightless spring of stiffness k, a damper with damping coefficient c (Figure 1a, b). The external dynamic loading producing the response $y(t)$ of the system is the time varying force $f(t)$, where t is time. $f_a(t)$, $f_s(t)$, and $f_d(t)$ in Figure 1(b) are time varying inertia, spring, and damping forces, respectively.

The differential equation governing the response of the SDOF system subjected to harmonic input, $f(t) = f_0 sin\bar{\omega}t$, with the forcing frequency $\bar{\omega}$, is given by (Biggs 1964; Clough and Penzien 1995):

$$m\ddot{y} + c\dot{y} + ky = f_0 sin\omega t \quad (6)$$

f_0 is the amplitude of the forcing function, $f(t)$ and a single dot on top of a character represent its 1st time derivative and the two dots represent 2_{nd} derivative. The dynamic magnification factor (DMF) for the steady-state response of the system is given by:

$$\text{DMF} = \frac{y_{dyn}}{(y_{st})} = \frac{1}{\sqrt{[1-\beta^2]^2+[2\xi\beta]^2}} \quad (7)$$

where, y_{dyn} and y_{st} are, respectively, the maximum dynamic and maximum static responses of the mass, in which $y_{sta} = \frac{f_0}{k}$; β is the frequency ratio given by $(\bar{\omega}/\omega_n)$, ω_n is the undamped natural frequency of the system and is equal to $(k/m)^{1/2}$, and ξ is the damping ratio given by given by $\xi = \frac{c}{c_c}$. Here c is the actual damping and c_c is the critical damping given by $c_c = 2m\omega_n$.

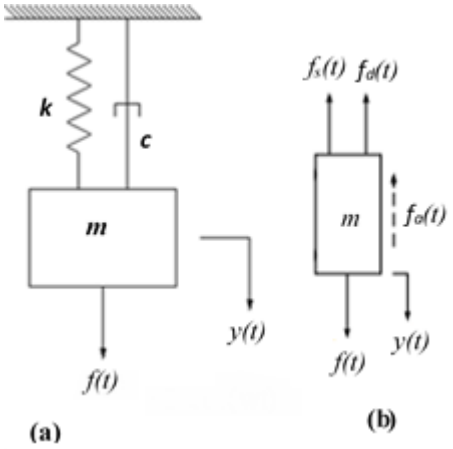

FIGURE 1. Idealized SDOF system: (a) basic components (mass-spring-damper system); (b) forces in equilibrium.

Figure 2 shows the plot of DMF versus the frequency ratio, β. It can be seen from Figure 2 that DMF varies with the frequency ratio ($\beta = \omega/\omega_n$) and the damping ratio (ξ). If the frequency ratio is small (i.e., the force is slowly varying), the response is in phase with the input force, DMF is only slightly larger than 1 and the response does not changes with the change in damping of the system. But when the forcing frequency is close to the natural frequency of the system (i.e., $\beta \sim 1$), DMF can be quite large. From Eq. (7), if can be seen that for undamped system the response would be infinite if $\beta = 1$ (i.e., if the system's natural frequency is equal to the forcing function or loading frequency). This phenomenon is called resonance.

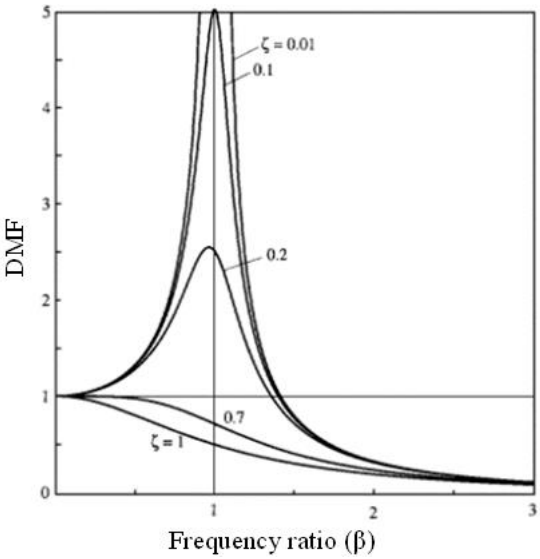

FIGURE 2. Plots of dynamic magnification factor for a damped system excited by harmonic force (Clough and Penzien 1995).

The concept presented above is for a single degree of freedom system. In a real life scenario, the damping is never zero; hence, the DMF will never be infinity. Also, a structure in real life will have more than one degree of freedom and hence multiple modes of the system might be excited by the external force and there may be secondary modes of vibration that will add to the primary mode deformations of mode. The phenomenon of resonance and dynamic amplification of the response of a bridge under a moving train load has been explained in the subsequent sections.

4.4.2 Theory Behind Moving Loads on a Beam

Consider a straight, non-uniform beam AB (Figure 3) with flexural stiffness $EI(x)$, length L, and mass per unit length $m(x)$. Note that E is modulus of elasticity; I is moment of inertia of the beam cross section; and x is distance measure from left end of the beam. The transverse loading $F(x,t)$ is assumed to vary arbitrarily with position and time. The transverse displacement $y(x,t)$ is a function of these variables.

The governing partial differential equation of motion to determine the transverse displacement $y(x,t)$ for the beam can be written as (Biggs 1964; Clough and Penzien 1995):

$$\frac{\partial^2}{\partial x^2}\left[EI(x)\frac{\partial^2 y(x,t)}{\partial x^2}\right] + m(x)\frac{\partial^2 y(x,t)}{\partial t^2} = F(x,t) \qquad (8)$$

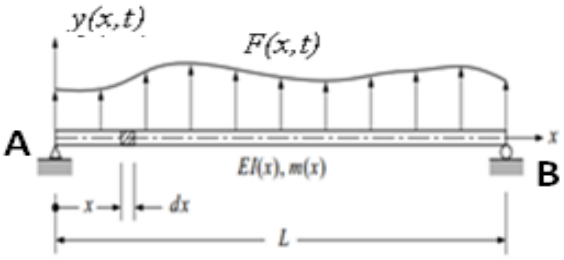

FIGURE 3. Basic beam subjected to dynamic loading (Clough and Penzien 1995).

For the moving load analysis, the forcing function $F(x,t)$ needs to be expressed appropriately. Several analytical studies can be found in literature in which the moving vehicle is represented by a single force or single degree of freedom system. For example, the dynamic response of a beam under a moving vehicle using the analytical solution has been presented by Biggs (1964) considering the vehicle traveling with a constant speed and representing it by four different models, namely (a) a constant moving force, (b) a rolling mass, (c) a sprung mass system, and, (d) a spring mass damper system.

The analysis of the real life railroad bridges traversed by actual trains, however, is much more complex problem. The train consists of many cars and each car has multiple axles through which the train load is transferred to the bridge. Therefore, in reality, it is not a single-degree-of-freedom system. Moreover, the train also undergoes vibration as it moves over the train and, therefore, there is interaction between the bridge and the vehicle motion (e.g., Dhar et al. 1978; Chu et al, 1979; Yang et al 2004; Fryba 2013). However, for practical purposes, a good approximation of a moving train over a bridge has been modeled as a series of axle loads moving over a bridge (Yong et al.1997; Xia et al.2006; Yoon et al.2013).

Railroad bridges are subjected to a resonance phenomenon, a condition when the loading frequency matches with one of the natural frequencies of the bridge. When there is no damping or very less damping in structure, the response of the bridge increases gradually with each additional train axle passing over the bridge. The resonance phenomenon of the bridge-train system is mainly affected by natural frequency of the bridge, the vehicle load, and its axle arrangement. Xia et al. (1996), Yang et al. (1997), and Yoon et al. (2013) studied the resonance phenomenon considering the bridge as a simply supported beam of span length l_b traversed by a train, represented by a series of concentrated constant loads of magnitude P at constant interval d_v (Figure 4). The train contains identical cars each of full length l_v, l_c as a distance between the two bogies of a car, and distance l_w between the two wheel-axles of a bogie.

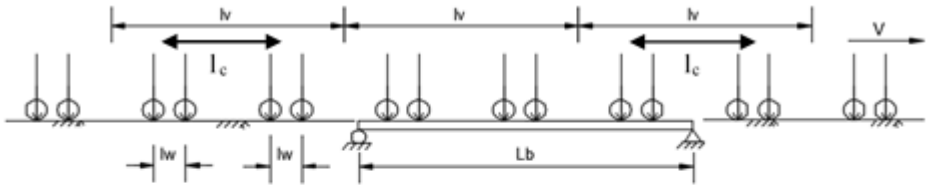

(a) Train axles moving over a bridge.

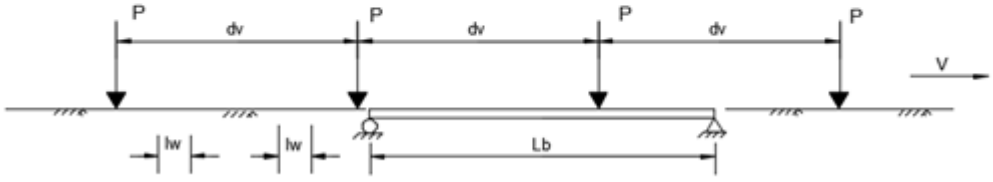

(b) Series of concentrated constant moving loads.

FIGURE 4. Bridge with series of (a) train axles, (b) concentrated constant loads, moving at constant velocity (Xia et al. 2006).

The equation of motion of the beam under the action of a series of concentrated moving loads, *P*, travelling at a uniform speed, *V*, can be obtained from Eq. 8 by replacing the forcing function *F*(*x*,*t*) with that corresponding to the series of concentrated moving loads as (Xia et al. 2006):

$$EI\frac{\partial^4 y(x,t)}{\partial x^4}+\overline{m}\frac{\partial^2 y(x,t)}{\partial t^2}=\sum_{k=0}^{N-1}\delta\left[x-V\left(t-\frac{k.d_v}{V}\right)\right]P, \tag{9}$$

where $y(x, t)$ is the displacement of beam at a position x at time t; δ is the Dirac delta function; E is modulus of elasticity; I is moment of inertia of the beam cross section; $\overline{m}$ is the constant mass per unit length of the beam; N being the total number of moving loads; and k varies from 0 to N corresponding to each moving load.

Using the mode superposition method, the dynamic deflection of the beam may be represented by the summation of the modal components as:

$$y(x,t)=\sum_1^n A_n\,\phi_n(x) \tag{10}$$

where A_n is the modal amplitude (which varies with time, t); and $\phi_n(x)$ is the characteristic mode shape, which is only a function of location, x.

Considering only the first mode of vibration, the displacement at any position of the beam for a particular time can be written as:

$$y(x,t)=A_1(t).\phi_1(x) \tag{11a}$$

$$\text{where}\quad A_1(t)=\frac{2PL^3}{EI\pi^4}\frac{1}{1-\beta^2}\left[\sum_{k=0}^{N-1}\sin\overline{\omega}\left(t-\frac{kd_v}{V}\right)-\beta\sum_{k=0}^{N-1}\sin\omega_n\left(t-\frac{kd_v}{V}\right)\right] \tag{11b}$$

and $\phi_1(x)=sin(\frac{\pi x}{L_b})$ is the characteristic mode shape.

Here, $\beta=\frac{\overline{\omega}}{\omega_n}$ is the ratio of requency of excitation to the natural frequency of the beam, and $\frac{1}{1-\beta^2}$ is the dynamic amplification factor, $\overline{\omega}=\frac{\pi V}{Lb}$ is the frequency of excitation/loadings, and $\omega_n=\frac{\pi^2}{{L_b}^2}\sqrt{\frac{EI}{\overline{m}}}$ is the natural frequency of the beam (bridge). Finally, Eq. (11a) can be written as:

$$y(t)=\frac{2PL^3}{EI\pi^4}\frac{1}{1-\beta^2}\sin\left(\frac{\pi x}{L_b}\right)\left[\sum_{k=0}^{N-1}\sin\overline{\omega}\left(t-\frac{kd_v}{V}\right)-\beta\sum_{k=0}^{N-1}\sin\omega_n\left(t-\frac{kd_v}{V}\right)\right] \tag{12}$$

The first term of Eq. (12) is the forced response of the beam due to the moving loads and the second term the transient response due to the free vibration of beam. The resonant response of the beam can be divided into two types, corresponding to each of these responses as presented in the following sub-sections

4.4.3 Resonance in Beam Caused by Moving Loads

(*a*) *Resonance under transient response:* According to Xia et al. (2006) obtained the resonance condition of vibration of the bridge under moving load series corresponding to the transient response [second term in the right hand side of Eq. (12)] can be found (considering all modes) as:

$$\omega_n d_v/2V=i\pi \quad (i=1,2,3,\ldots) \tag{13}$$

Noting $\omega_n = 2\pi f_{bn}$, the resonant condition given by Eq. (12) can expressed as (Xia et al 2006):

$$V_{br}=\frac{3.6 f_{bn} d_v}{i}\ (n=1,\,2\ldots,\ i=1,\,2\ldots.) \tag{14}$$

where V_{br} = resonant speed of train; f_{bn} = nth mode natural frequency of the bridge; d_v is interval of the moving loads; and multiplier i = 1, 2… is based on the extreme condition.

Eqs. (13) and (14) show that when a train with regularly arranged vehicle wheel axles moving at a speed V, the bridge resonance occurs when the loading period (d_v/V) is close to the nth natural vibration period ($2\pi/\omega_n$) of the bridge, and that

a series of resonant responses related to different bridge natural frequency may occur corresponding to different train speeds. This resonant condition derived from the transient response is called as the first resonant condition of the bridge. A series of resonant responses related to different bridge natural frequency may occur corresponding to different train speeds.

(b) Resonance under the steady state response: From the steady state response part (first term in the right hand side) of the Eq. 12, which represents the forced response of the bridge (beam), a different (second) resonant speed can be obtained by simply equating loading frequency $\overline{\omega}$ equal to the structural natural frequency ω_n. For a simply supported beam of length L_b the loading frequency is given $\overline{\omega} = n\pi V/L_b$ and the nth natural frequency of the beam $\omega_n = 2\pi f_{bn}$, the resonant train speed is given by:

$$V_{br} = \frac{7.2\, f_{bn} L_b}{n} \qquad (n = 1, 2...) \qquad (15)$$

This condition obtained from the steady state (forced) response is called as the second resonant condition of the bridge (Lu et al. 2012). It should be noted that it is very rare for this condition of resonance (second resonant) to occur in the bridge as it requires the train to move over the bridge at very high speed. For example, if the first natural frequency of the bridge is 1.256 Hz with span length 67 m (219.8 ft) (similar to the bridge studied in this project), the first resonant speed is 596.8 km/h (370 mph), which is not practically possible at the current time. Hence, the resonance of the bridge under this condition has not been considered in this study.

Later in this report, the resonant speeds in vertical and lateral direction for Amtrak Acela, Amtrak Regional and Metro–North M8 trains on Devon Bridge were determined and analyzed using the finite element and analytical relations and compared with the resonant speeds calculated using Eq. (14).

FIGURE 5. Span 7 of Devon railroad drawbridge, Milford, Connecticut.

4.5 RAILROAD BRIDGE STRUCTURE SELECTED FOR STUDY

Open deck trusses are an extremely common railroad bridge design nationwide, especially for spans greater than roughly 150 feet. The open deck truss railroad bridge span selected for this research study, described below, is typical of these bridges nationwide, including those corridors designated for upgrade for high speed passenger operation, especially the Northeast Rail Corridor between Washington, D.C. and Boston, Massachusetts.

The bridge selected for this research study was the Devon railroad bridge, spanning the Housatonic River between Stratford (on the west) and Milford (on the east) in Connecticut, shown in Figures 5 and 6. The Devon railroad bridge is a 325.2 m (1,066 ft 10 in.) long, open deck, two track, steel through truss composed of two identical, and side-by-side

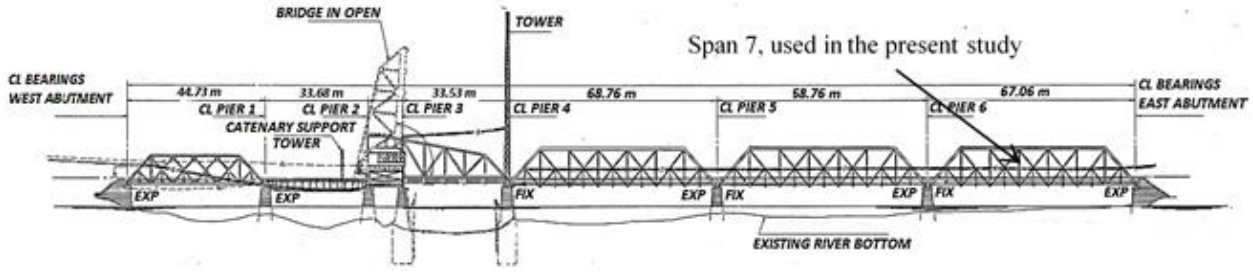

FIGURE 6.- Elevation view of Devon Bridge, facing upstream (north).

parallel independent bridge structures (north and south bridges), sharing only abutments and piers. Each bridge consists of series of seven spans (five through-truss spans and two deck girder spans) separated by approximately 1.83 m (6 ft). One of the through-truss spans in each bridge is a Scherzer rolling lift bascule, to allow marine traffic to pass the bridge. Figure 6 shows an elevation view of the Devon Bridge, facing north (upstream). For this research project, span 7, the easternmost span adjacent to the abutment of the north bridge, was selected for the research investigation. Figure 7(a) shows the schematic arrangement of all the principle members of the span 7 truss. This truss span consists of seven panels of 9.47 m (31 ft 1 in.), total length centerline to centerline of bearings, 66.32 m (217 ft 7 in.), and weighs approximately 3,298 kN (741.43 kips). Figures 7(b), (c), (d), and (e) show the typical section of stringer, floor beam, vertical, and top chord, respectively. All research was conducted on span 7, the easternmost span of the north bridge.

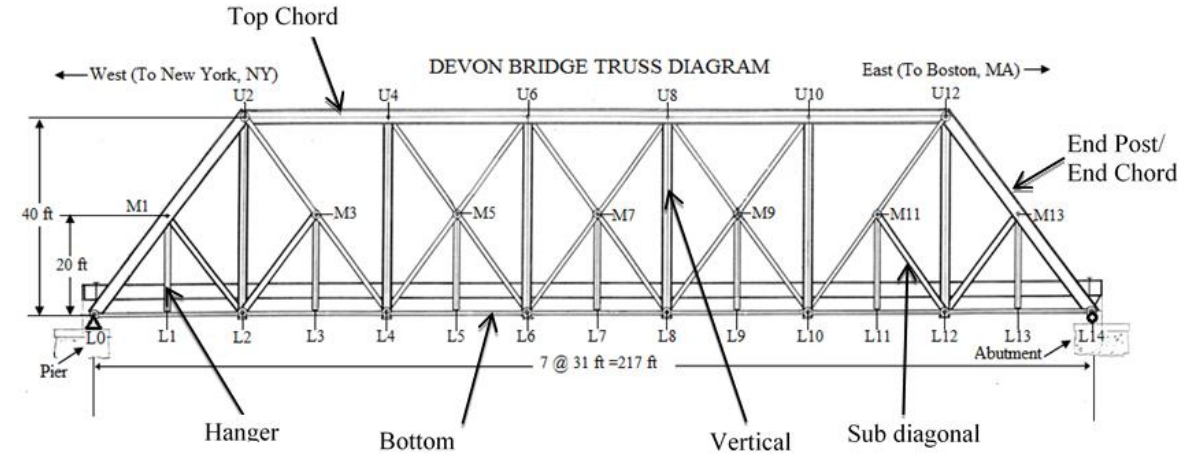

(a) Schematic arrangement of the members of the Devon bridge, span

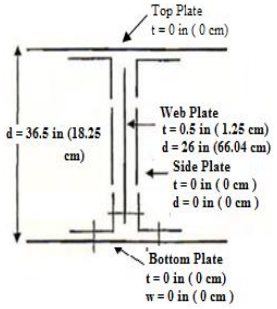

(b) Typical section of stringer.

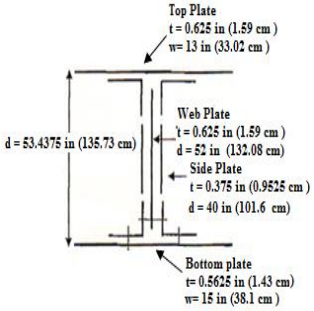

(c) Typical section of intermediate floor beam.

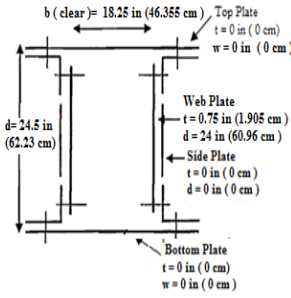

(d) Typical section of vertical L2-U2.

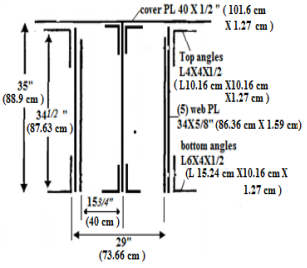

(e) Section view of top chord U2-U4.

FIGURE 7. Schematic arrangement of the principal members of the Devon Bridge, span 7, and typical sections of stringer, floor beam, vertical and top chord.

4.6 FINITE ELEMENT MODEL AND ANALYSIS

4.6.1 Theory Behind Finite Element for Structural Dynamics

For the finite element analysis, the dynamic equations of motion for a multi-degree-freedom structure, such as the bridge studied for this research, can be expressed in a matrix as shown here:

$$[M]\{\ddot{y}\} + [C]\{\dot{y}\} + [K]\{y\} = \{F(t)\} \tag{16}$$

where [*M*], [*C*], and [*K*] represent the mass, damping, and stiffness matrices of the structure, respectively; {*F*(*t*)} is the external load vector; and {*y*} is the vector of degrees of freedom (displacements and rotations) at the discrete points of concern. A dot on top of a character represents its time derivative.

The sizes of the mass, stiffness, and the damping matrices correspond to the degrees of freedom for the Devon Bridge span considered. The train load coming into the bridge structure corresponds to the external load vector {*F*(*t*)} as presented in Eq. (16). While the mass, stiffness, and damping matrices of the bridge are constant, the load vector changes with the type and speed of trains considered.

4.6.2 Finite Element Models of the Devon Railroad Bridge Span Studied

A detail FEM of span 7 of the Devon railroad bridge was developed using STAAD.Pro finite element software, code by Bentley Systems, Inc. (2012). Beam and truss elements were utilized in preparing the FEM with the boundary conditions as representative of the actual truss system. The FEM of the entire span 7 truss bridge structure included altogether 5,316 elements and 4,371 nodes. Various members/components/parts of the Devon Bridge span, their number, the corresponding FE element type, and number of FE nodes and elements in each member are shown in Table 1. The bridge span was modeled with hinge support in one end and roller support at the other. Figure 8 shows the FEMs of various components (Figure 8a, b) and the full structure (Figures 8c, d) of span 7 of the Devon Bridge.

Two different FEMs of the Devon Bridge were constructed. The first model had simplified top bracings and the second model, which was as a result of an update based on the field tests, had detailed top-bracings. Figures 8(c) and 8(d) show the FEM of Devon Bridge with simplified top bracings and detailed top bracings, respectively. The simplified model was created with the intent of saving computational time and the responses of these two models were compared with verify the accuracy of the simplified model. The comparison of the response between the two models is shown later in Figures 15 and 16 and Table 6.

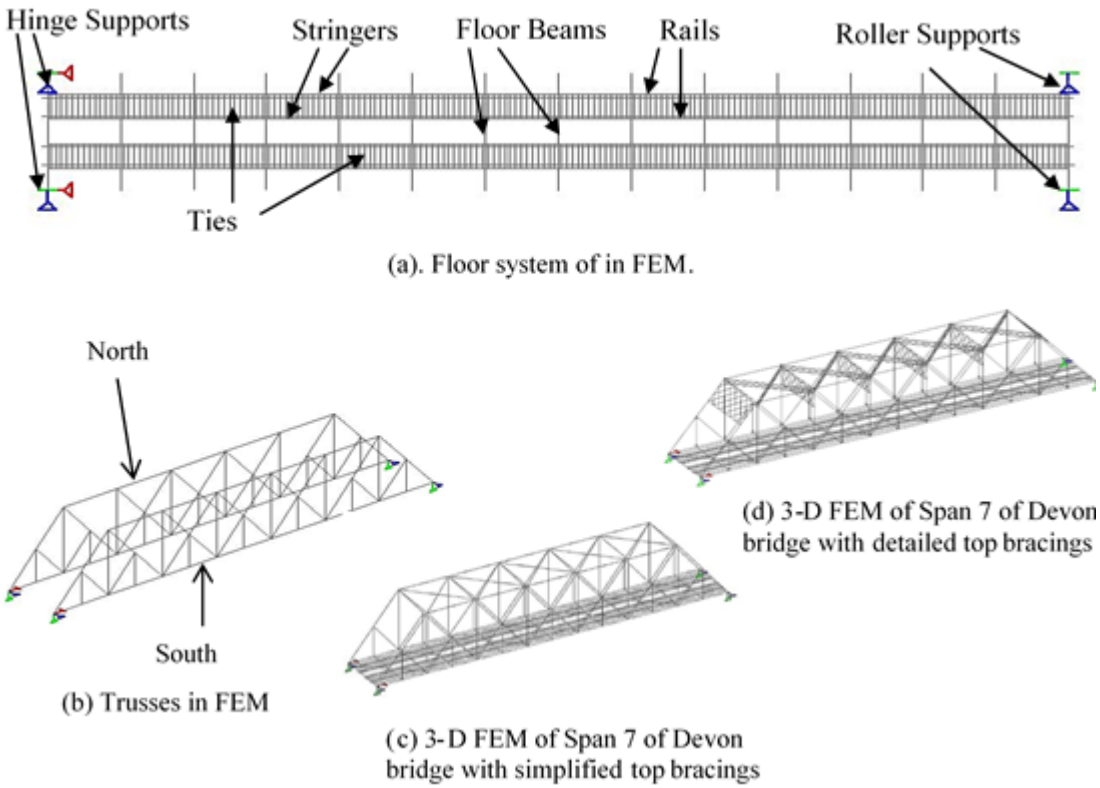

FIGURE 8. Components of the FEM and two different FEM models of span 7 of Devon Bridge.

TABLE 1. Various components/parts of Devon Bridge, their number, element type, number of elements, and nodes for FE analysis

SN	Components/Members	Number of members	Element Type for FE analysis	Number of Nodes in each member type	Number of Elements in each member type
1	Floor beam	15	Beam	40	39
2	Stringer	56	Beam	10	9
3	Ties	364	Beam	4	3
4	Rails	4	Beam	184	183
5	Truss-Vertical post	12	Beam	40	39
6	Truss-End Chord	8	Beam	20	19
7	Truss-Hangers	14	Beam	20	19
8	Truss-Bottom Chords	14	Truss	2	1
9	Truss-Top Chords	10	Beam	20	19
10	Truss- Intermediate Struts	6	Truss	2	1
11	Truss-Diagonals	40	Truss	2	1
12	Truss- Cross Bracings	10	Truss	2	1
13	Truss-bottom bracing	28	Truss	2	1
14	Truss-cross bracing	28	Truss	2	1
Total number of nodes in the Finite Element model of the entire structure					4371
Total number of elements in the Finite Element model of the entire structure					5316

4.6.3 Description of Passenger Trains Used for Finite Element Analysis

Devon Bridge is used by Amtrak (Acela and Regional) and Metro–North passenger trains for crossing the Housatonic River between Milford and Stratford in Connecticut. The axle arrangements and axle loads of these passenger train considered for this study are shown in Figure 9 (a, b, c). The train axle loads shown in Figure 9 do not include the additional load due to passengers. The percentage increase in axle load for fully loaded train cars compared with the empty train cars can be as high as 12% for Metro–North passenger trains, while for Amtrak Acela the increase in percentage of axle load is only approximately 8.5%. Unless otherwise noted, for this research an Amtrak Acela train with two engines (one at each end) and six cars in between; Amtrak Regional train with one front engine and eight cars; and Metro–North M8 train with eight cars have been considered. However, the number of cars can vary as the trains usually have more cars during the peak hours and fewer cars during other times. The maximum permissible speed limit of the passenger trains on the bridge was 64.37 km/h (40 mph).

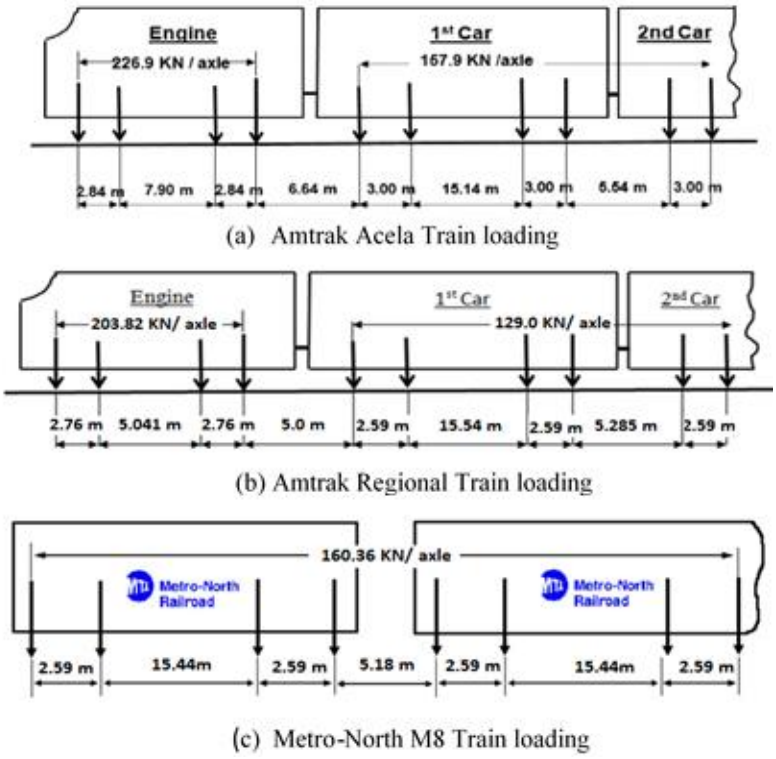

FIGURE 9. Axle arrangements and loads of passenger trains: Amtrak Acela, Amtrak Regional, and Metro–North M8.

4.6.4 Dynamic Train Load for Finite Element Analysis

The dynamic (moving) train loading for finite element analysis to obtain bridge response was determined based on the axle loading and axle spacing of each train type as shown in Figure 10 (a, b, c, and d). Each train's wheel load time history (F vs. t) was modelled as a triangular pulse, shown in Figure 10 (b). The ramp time, Δt,, the difference between time t_2 and t_1 or time t_3 and t_2, for each wheel load, was determined from the distance, d, between the two consecutive nodes in the FEM of the rail and the speed, V, of the train (i.e., $\Delta t = d/V$; see Figure 10a).

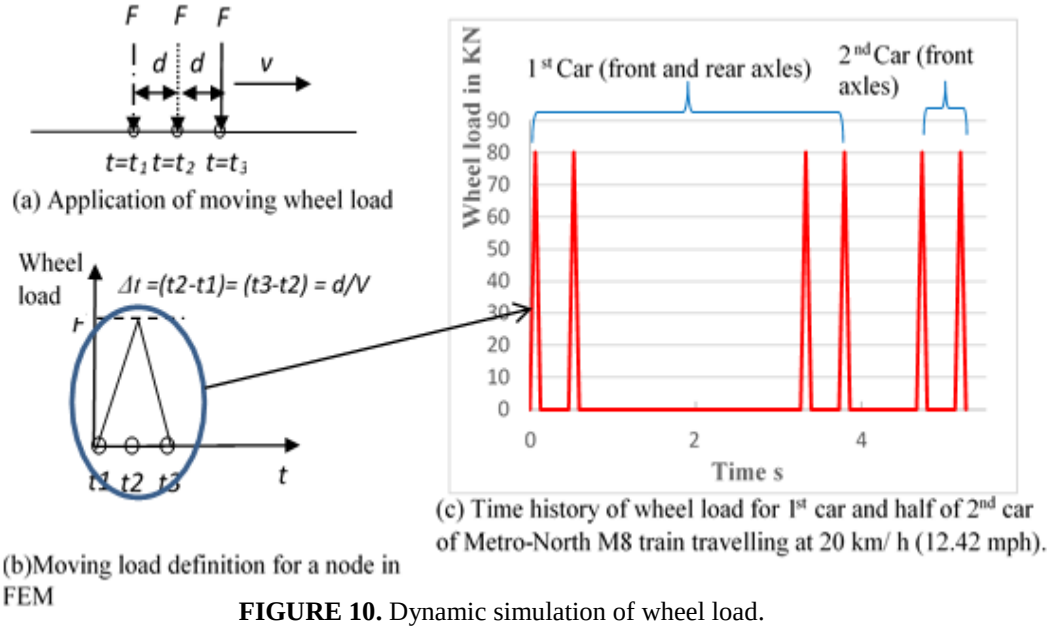

FIGURE 10. Dynamic simulation of wheel load.

The axle loading versus time curve for a train at a given speed was determined combining all the wheel loads of the train. Figure 10 (c) shows the load versus time curve for the front two and the rear two axles of the first car and the front two axles of the second car.

Figure 11 shows the load versus time curve for the Metro–North M8 train with eight cars travelling at 20 km/h (12.42 mph). Based on the distance between consecutive nodes and the speed of the trains, different arrival times for the time vs. load curve were defined for each node to simulate the moving load.

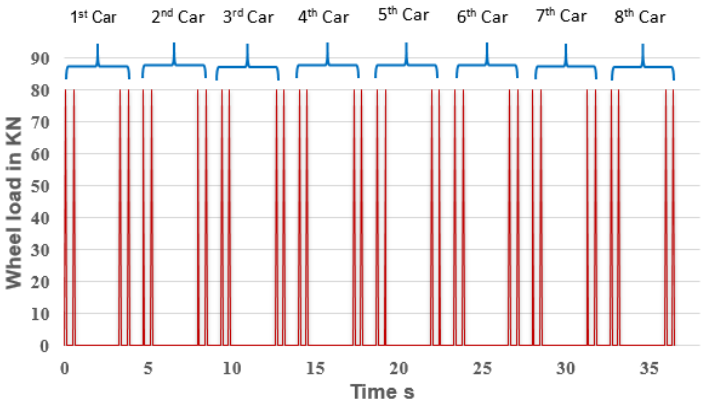

FIGURE 11. Time history of wheel load for Metro–North M8 train with eight cars travelling at 20 km/h (12.42 mph).

4.6.5 Moving Load Static Analysis Model (Static Influence Line Technique)

To simulate the vehicle moving load condition for static analysis, the axle loads of the trains travelling westbound (toward New York) on track 3 (north track) were moved from one end of the bridge to other at a total of 100 discrete steps. That is, the loads were moved (advanced forward) by 65 cm (2.17ft) increments in each load case. Static analysis was performed at each load step and the response of the bridge was obtained at each step.

The static response (vertical displacements) of node L7 and L8 of north truss under Acela and Regional train on track 3 moving westbound (toward New York) is shown in Figures 12 and 13, respectively. The results in Figure 12 show two larger peaks of displacements at two ends of the displacement spectrum for the Acela train. This is consistent with the fact that the Amtrak Acela train has two engines, one at each end, with much larger axle loads than the coach cars in between. Similarly, there is a single larger peak displacement (Figure 13) under the Amtrak Regional train due to the engine being only at the front of the train. Also, for both trains, hanger node (L7) has a higher displacement than bottom chord node (L8) (Refer to Figure 7 for the locations of these nodes.)

Tables 2 and 3 show the vertical and lateral displacement results (maximum values), respectively, at various locations. It can be seen as expected that the displacement of nodes of the north truss adjacent to track 3 has higher vertical displacement due to closer proximity of the vehicle loads than that of the similar nodes on opposite south truss further from track 3.

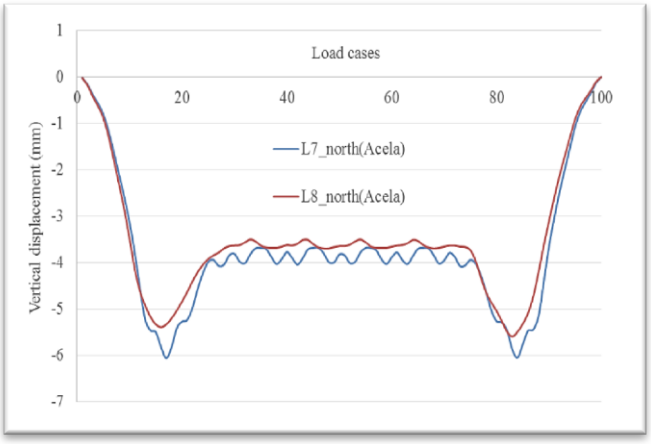

FIGURE 12. Static displacement of North Truss nodes L7 and L8 from Amtrak Acela train on track 3.

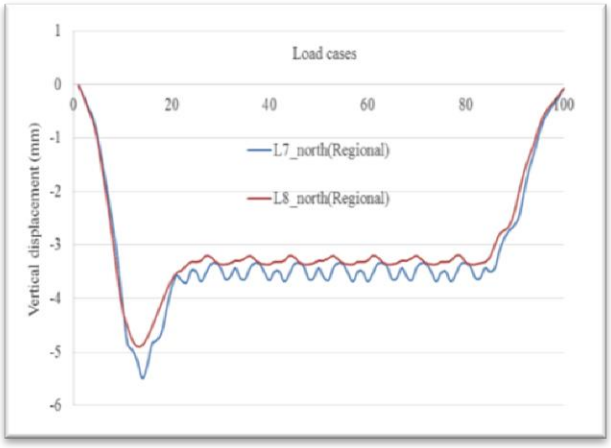

FIGURE 13. Static displacement of North Truss nodes L7 and L8 from Amtrak Regional train on track 3.

TABLE 2. Vertical displacement of bridge under sets of static train loads moving toward New York on track 3

Trains	Truss Nodes—Vertical Displacement (mm)									
	L6		L7		L8		U6		U8	
	North Truss	South Truss	North Truss	South Truss	North Truss	South Truss	North Truss	South Truss	North Truss	South Truss
Amtrak Acela	6.97	4.35	7.22	4.71	6.75	4.33	7.03	-0.27	6.87	-0.19
Amtrak Regional	7.76	3.49	7.84	3.57	7.57	3.42	7.85	3.48	7.62	3.44
Metro–North M8s	2.29	3.3	7.68	3.44	7.36	3.28	7.39	3.31	7.45	3.3

Conversion factor: 1 mm = 0.04 in.

TABLE 3. Lateral displacement of bridge under sets of static train loads moving toward New York on track 3

Trains	Truss Nodes—Lateral Displacement (mm)									
	L6		L7		L8		U6		U8	
	North Truss	South Truss	North Truss	South Truss	North Truss	South Truss	North Truss	South Truss	North Truss	South Truss
Amtrak Acela	0.44	0.45	0.52	0.51	0.52	0.51	4.76	4.64	3.98	3.8
Amtrak Regional	0.46	0.47	0.53	0.534	0.54	0.55	3.37	3.26	3.01	2.91
Metro–North M8s	0.4	0.4	0.47	0.46	0.48	0.48	2.95	2.83	2.65	2.53

Conversion factor: 1 mm =0.04 inches

4.6.6 Modal Analysis Frequencies and Mode Shapes

Modal analyses of the bridge span to determine frequencies and mode shapes of both simplified top bracing (Figure 8c) and detail top bracing (Fig. 8d) models were performed. A total of 50 frequencies and mode shapes were obtained. Due the existence of a number of eyebars/diagonal members and rails, which are relatively flexible, most of the frequencies and modes were local modes. This is true especially for the detail bracing model of the bridge structure. The natural frequencies and respective mode numbers for the first four global modes of the bridge are shown in Table 4.

TABLE 4. First four global modes and corresponding modal parameters of both simplified and detailed bracing FE models

.

Global Mode	Simplified Model			Detailed Model			Difference in frequencies (%)
	Mode No.	Frequency (Hz)	Time Period(s)	Mode No.	Frequency (Hz)	Time Period(s)	
1st Lateral	1	1.256	0.796	5	1.478	0.0.677	−17.68
2nd Lateral	10	3.635	0.438	19	3.558	0.281	2.12
1st Vertical	14	4.854	0.206	32	4.843	0.206	0.23
1st Longitudinal	17	7.681	0.130	50	7.739	0.129	−0.76

It can be seen from the frequency results that except for the first lateral mode, the global natural frequencies obtained from both FEMs are extremely close. The first four global mode shapes obtained from the FE modal analysis of the bridge span for the simplified top bracing models are shown in Figure 14 (a–d).

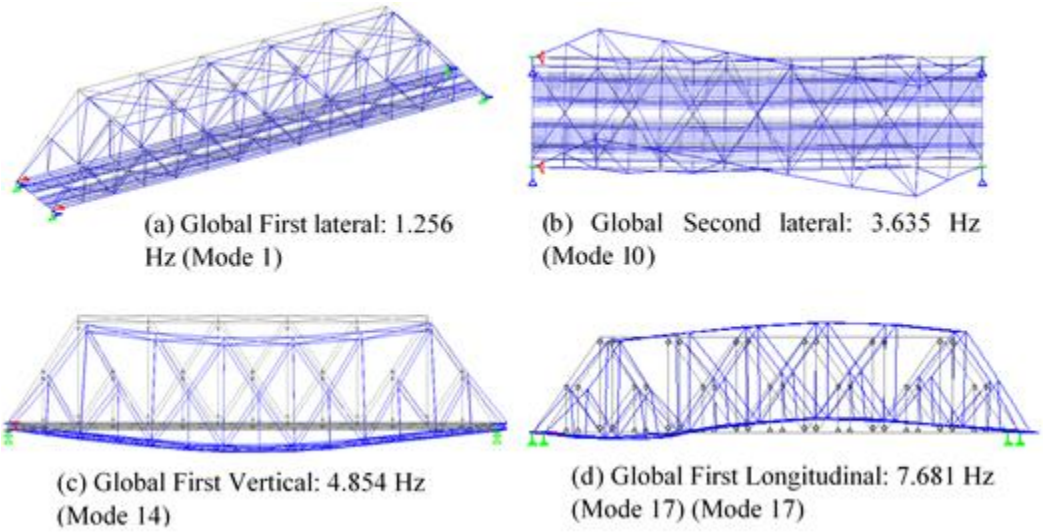

FIGURE 14. First four global modes of vibration from FEM (simplified top-bracing model).

4.6.7 Dynamic (Time History) Analysis and Results Using Finite Element Model

The dynamic (time history) analysis of the bridge under the moving trains was performed using the finite element method and the dynamic displacement response of the bridge was obtained. The dynamic loading from the moving vehicle for the finite element analysis was determined utilizing the method described above in section "Dynamic Train Load for Finite Element Analysis." The trains were considered moving on track 3 toward New York (similar to a field test on the actual bridge) at various speeds. Although a multi-degree structure has as many modes of vibration as the degrees of freedom considered for the analysis, not all modes will have significant effect/contribution in determining the dynamic response of the bridge. Moreover, different train speeds will excite different modes/frequencies of vibrations. Therefore, when using the mode superposition method, as is the case in the current study, it is important to consider the adequate number of modes in the computation of the dynamic response of the bridge, so that the results obtained can be closer to the actual values. Considering a higher number of modes will obviously produce greater accuracy of results. However, it can be computationally prohibitive. For the structure and FEM considered in this study, a verification study was done first by computing the dynamic response for a couple of train loadings by taking several numbers of modes. It was found that the response of the bridge obtained by considering a number of modes more than 50 did not differ significantly from that with 50 modes. Hence, only modes 1 through 50 were considered to generate/obtain dynamic response results.

The maximum vertical and lateral displacements of several locations of the bridge under various trains traveling on track 3 obtained from the time history analysis using STAADPro finite element code (Bentley 2012) are shown in Tables 5 and 6, respectively.

TABLE 5. Maximum vertical displacement of bridge from the FEM time history analysis

Trains	Truss Nodes—Maximum Vertical Displacement (mm) at 64.37 km/h (40 mph)									
	L6		L7		L8		U6		U8	
	North Truss	South Truss	North Truss	South Truss	North Truss	South Truss	North Truss	South Truss	North Truss	South Truss
Amtrak Acela	9.47	4.54	9.64	4.83	9.52	4.51	9.6	4.55	9.61	4.53
Amtrak Regional	8.19	3.76	8.29	3.7	7.8	3.6	8.28	3.75	7.89	3.63
Metro–North M8s	7.9	3.76	8.29	3.88	8	3.75	8.03	3.79	8.11	3.78

Conversion factor: 1 mm = 0.04 in.

TABLE 6. Maximum lateral displacement of bridge from the FEM time history analysis

Trains	Truss Nodes—Maximum Lateral Displacement (mm) at 64.37 km/h (40 mph)									
	L6		L7		L8		U6		U8	
	North Truss	South Truss	North Truss	South Truss	North Truss	South Truss	North Truss	South Truss	North Truss	South Truss
Amtrak Acela	0.69	0.69	0.76	0.78	0.78	0.79	5.11	4.98	4.61	4.49
Amtrak Regional	0.64	0.65	0.73	0.72	0.74	0.75	4.22	4.1	3.76	3.65
Metro–North M8s	0.47	0.47	0.52	0.52	0.53	0.54	3.34	3.23	2.96	2.85

Conversion factor: 1 mm = 0.04 in.

Some more representative results from the dynamic analysis using the FEM have been presented in later sections, along with the field test results (see Figures 33, 34, 36, and 37).

4.6.8 Comparison Between the Two Finite Element Models of Devon Bridge: Simplified and Detailed Top-Bracing Models

The responses obtained from the simplified top-bracing and detailed top-bracing models of Devon Bridge span 7 as shown in Figures 8 (c) and 8(d) are compared in this section.

4.6.8.1 Static moving load responses

The responses obtained from simplified and detailed top-bracing models of the bridge span under a train load using static live load analysis methods were compared. The vehicle wheel load was moved starting from the east end to the west end (Boston to New York) over the bridge span on track 3 at a total of 100 discrete steps. The static response of the bridge for each location of the train was obtained for both FEM. The displacements of the bottom chord node L7 and the stress in member M7–L8 in the north truss of the bridge span analyzed under Amtrak Acela train on track 3 for both models are presented in Figures 15 and 16, respectively. It can be seen from these figures that the vertical displacement of node L7 and the axial stress in member (M7–L8) for both bracing models are very close to each other, with the vertical displacement of the model with detailed bracings being slightly smaller than the one with simplified top bracings.

4.6.8.2 Modal frequencies

From the results presented above under "Modal Analysis—Frequencies and Mode Shapes" section, the difference in 1st lateral mode is about 17.7%; however, the differences in 2nd lateral, 1st vertical, and 1st longitudinal modes are negligible. The discrepancy in the 1st lateral mode (higher value for the detailed top-bracing model) can be mainly attributed to the way the top-bracing system was modeled. In the simplified model, it was modeled by one single member with equivalent stiffness, whereas in the detailed model the bracing system had some depth that provided more rigidity for rotation and hence had added rotational stiffness in the lateral direction.

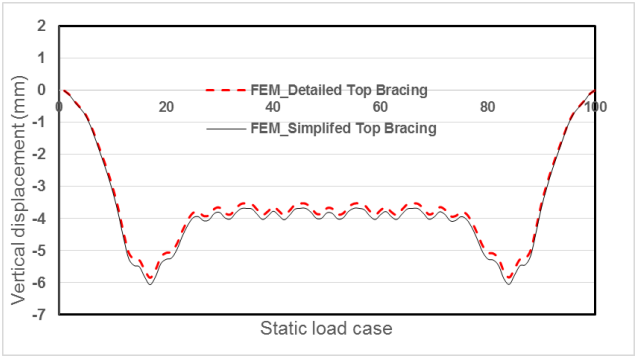

FIGURE 15. Vertical displacement of node L7 of north truss under Amtrak Acela train on track 3 moving toward New York City for both FE models.

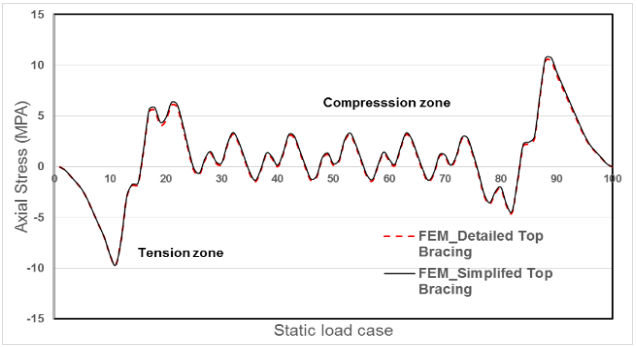

FIGURE 16. Axial stress diagram for member M7–L8 of north truss under Amtrak Acela train on track 3 moving toward New York City for both FE models.

However, since the present study was primarily focused on vertical effect/mode and that the frequencies and the displacements of both models were close in this direction, the simplified model was used for further finite element analysis in order to save the computational time.

4.7 FIELD TESTING AND DATA PROCESSING

4.7.1 Field Test Protocol and Data Collection

Data obtained from field tests on the bridge provide a reliable estimation of the dynamic characteristics of the bridge. The field vibration testing of span 7 of the Devon Bridge was performed under four types of passenger trains [Amtrak–Acela, Amtrak Regional; Metro–North M8 (electrical multiple units) and Waterbury (diesel engine and standard coaches)] to obtain the bridge response using different types of sensors: accelerometers, strain gages, and LVDTs.

The four types of trains used in the field testing were operated in both eastbound (toward Boston) and westbound (toward New York City) directions, at various speeds, up to the maximum allowable speed limit of 64.4 km/h (40 mph). On different occasions, non-revenue test trains were provided by both Amtrak and Metro–North, which were also operated at controlled speeds of 8.04, 16.09, 32.19, 48.28, and 64.37 km/h (5, 10, 20, 30 and 40 mph). Measurements were taken of vertical displacements at various bottom chord nodes (joints) and mid-points of floor beams and stringers using LVDTs. Strain gage measurements were taken at various hangers, verticals, diagonals, and end posts. Accelerometers were placed on top of the floor beams near the nodes (where the beam ends and vertical members were connected) to record vibrations in the vertical, lateral, and longitudinal directions. LVDTs were also used to record displacements in the longitudinal (x axis) and lateral (z axis) directions. Details of the recorded data are discussed later in this report. Sample field measured data as well as the deflection comparison between the FEM and field obtained data are also presented later in this report. A brief summary of the field testing dates, and the number of different types of trains and their speed range are shown in Table 7. For clarification when referring to track numbers, track 1 is the track adjacent to the south (downstream) truss and track 3 is adjacent to the north (upstream) truss on span 7 of the bridge.

It should be noted that several delays were encountered during the field test portion of this research project. First, bad weather on several dates caused the work to be cancelled. Because of safety considerations and the inherent dangers of working on an open deck bridge over water, work was occasionally cancelled because of either high winds, rain, cold temperatures, snow and ice, or a combination thereof. Second, because of other maintenance work being performed on the bridge by Metro–North, the railroad company was not able to provide access and the required flagman and other personnel on several dates the research team had selected for testing on the bridge. Third, the research team had to delay testing with both Amtrak and Metro–North non-revenue train sets (test trains), because of either non-availability of this equipment or non-availability of a crew. Thus, two 6-month-long, no-cost extensions for the project completion were required.

TABLE 7. Summary of field tests conducted at Devon Bridge

Date	No. of Trains and Speed Range	Amtrak Acela*	Amtrak Regional*	Metro–North M8*	Metro–North Water-Bury*	Total Trains
Aug. 12, 2014	No. of Trains	4	5	15	6	30
	Speed Range (mph)	35–40	37–40	10, 30–38	8–12	
Oct. 12, 2014	No. of Trains	2	1	3	1	7
	Speed Range (mph)	42–46	41	37–39	10	
Nov. 9, 2014	No. of Trains	1	2	6	2	11
	Speed Range (mph)	40	39–43	39–45	10	
Nov. 11, 2014	No. of Trains	6	4	18	3	31
	Speed Range (mph)	35-41	36-40	35-40	5-13	
Dec. 14, 2014	No. of Trains	2	5	15	3	25
	Speed Range (mph)	38	38–41	30–40	5–15	
Dec. 15, 2015	No. of Trains	5	2	7	2	16
	Speed Range (mph)	39–41	38–41	28–38	10-–14	
Aug. 29, 2015	No. of Trains	MN M8 Test Train (six coaches)				19
	Speed Range (mph)	5, 10, 20, 30, 40				
Dec. 5, 2015	No. of Trains	Amtrak Acela Test Train (2E + six coaches)				15
	Speed Range (mph)	5, 10, 20, 25, 30, 35, 40				
Dec. 6, 2015	No. of Trains	MN M8 Test Train (6 coaches)				19
	Speed Range (mph)	5, 10, 20, 25, 30, 40				
Dec. 12, 2015	No. of Trains	0	2	7	2	11
	Speed Range (mph)	N/A	42–45	40–44	10	

*Note: Number of coaches varies from train to train. Amtrak Acela had six to eight coaches, Amtrak Regional five to nine coaches, Metro–North M8 six to eight coaches, and Metro–North Waterbury three coaches.

4.7.2 Representative Field Test Data

Some representative sample field test results have been presented in this subsection. Figure 17 shows the typical accelerometer sensor locations on the bridge. Three accelerometers were located in stationary base stations (P2, P3, and P5) and two were located in movable stations (P1 and P4). The number within the parentheses of movable sensor locations, P1 and P4, represents the location corresponding to each setup of field experiment.

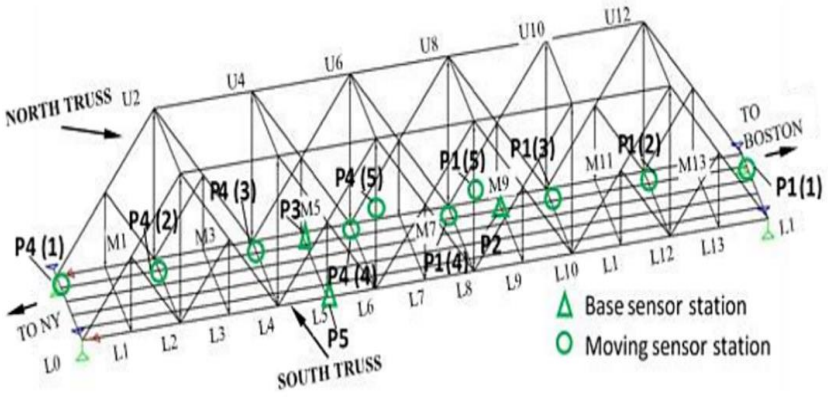

FIGURE 17. Accelerometer sensor location on the bridge.

A sample of one set of raw acceleration response data under a Metro–North M8 train in vertical, longitudinal, and lateral directions for accelerometer at location P2 obtained from the field testing is shown in Figure 18. It can be seen that the lateral acceleration signal is higher than acceleration signal for other two direction of the bridge.

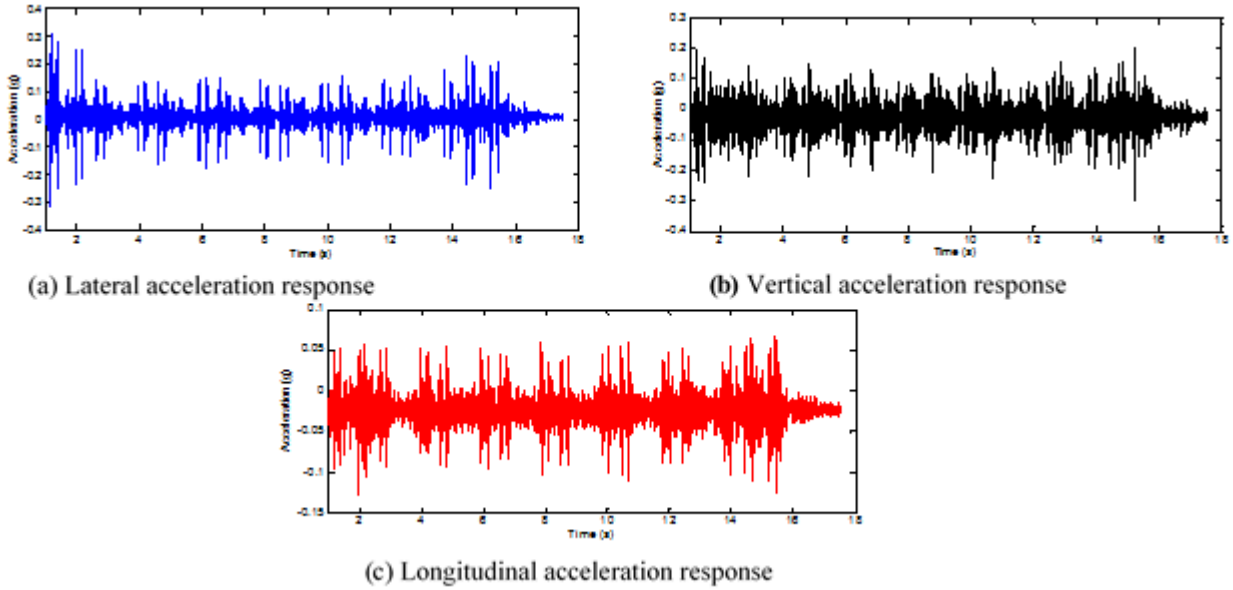

FIGURE 18. Field acceleration response in three directions for the bridge span under Metro–North M8 train for accelerometer at location P2.

Figure 19 shows the vertical displacement measured using an LVDT sensor at node L8 (bottom chord joint) of the south truss under an Amtrak Acela train moving at 8 km/h (5 mph) over the bridge on the south track (track 1). The vertical straight lines correspond to the axles of the train when they were right above the sensor location (node L8) to give the respective vertical displacement values (the intersection points of the vertical lines and the displacement curve) at that location, The horizontal (x) axis at the bottom represents the time after the first axle of the train has passed the start of the bridge and the x axis at the top gives the distance covered by the first axle from the entry point of the bridge. It can be seen in the graph that the maximum displacement is when the first set of axles (first engine) of the train is directly over the sensor location. Also, the displacements caused by engines (first and last peaks in the figure) are much higher than the displacements caused by the coaches (intermediate five peaks in Figure 19).

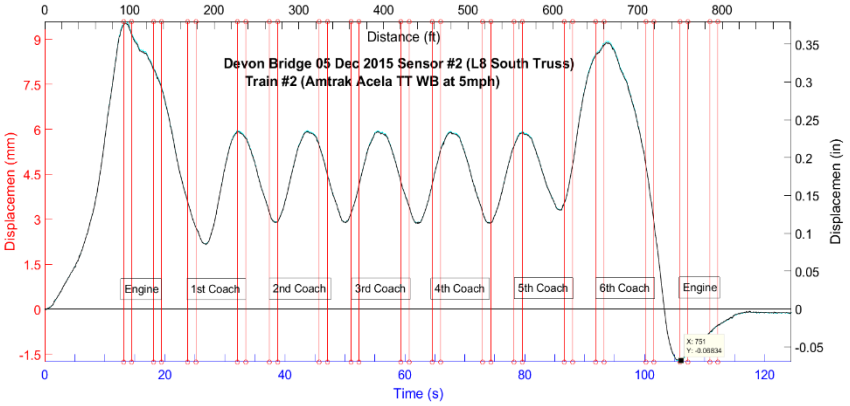

FIGURE 19. Vertical displacement of node L8 of south truss under Amtrak Acela train moving at 8 km/h (5 mph).

Figures 20 and 21 show the comparison of LVDT field measured displacement results of node L8 of south truss and north truss, respectively, under westbound Amtrak Acela test train

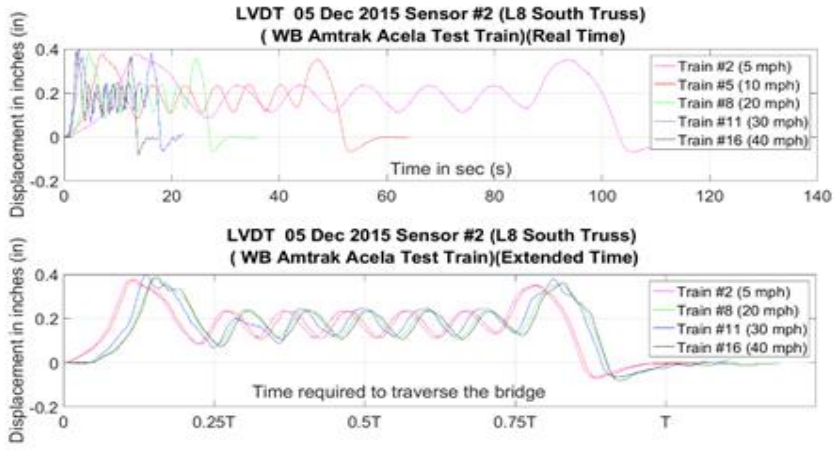

FIGURE 20. Vertical displacement comparison on node (joint) L8 south truss under west bound Amtrak Acela test train.

moving at five different speeds. The top sub-plot represents the actual displacement, whereas in the bottom sub-plot the data (bridge response recorded by accelerometer) have been stretched to overlap each other. Here, *T* used in the bottom sub-plots of both Figures 20 and 21 corresponds to the total time required by the train to make one complete pass of the bridge and varies for the different speed at which the train is moving. The values of *T* are approximately 120.4, 61.21, 32.05, 21.52, and 16.27 seconds for train travelling 8.04, 16.09, 32.19, 48.28, and 64.37 km/h (5, 10, 20, 30, and 40 mph), respectively. For this range of 8.0–64.4 km/h (5–40 mph) of the train speeds considered in the test, it is observed that the amplitude of displacement at joint L8 does not appear to change noticeably with speeds and the maximum displacement is caused by the engine. Figure 22 shows the strain readings on the top of the bottom flange of a running rail under the Amtrak Acela test train moving at different speeds as indicated in the plot.

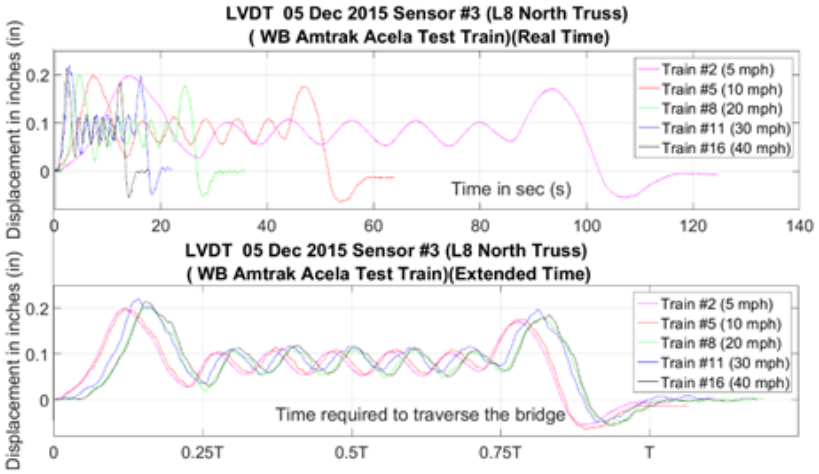

FIGURE 21. Vertical displacement comparison on node (joint) L8 north truss under west bound Amtrak Acela test train.

Figure 23 shows the comparison of strain readings on the adjacent diagonals connected (or framed into) the bottom chord nodes L2 and L12 (see Figure 7). These diagonals are (with all sensors attached to the top flange except for L2-M1, which is on the bottom flange): L2-M3 (south truss), L2-M1 (south truss), L12-M13 (south truss), L12-M13 (north truss), L12-M11 (south truss), and L12-M11 {north truss (refer to Figure 7)]. Each of these diagonals are built-up members, composed of two web plates and four angles (similar to those shown in the bottom portions of Figure 7). The results for diagonals framed into joint L2 are shown in the upper part of Figure 23, while for those connected to joint L12 are shown in the bottom part of the figure. As expected, the strains, and hence the stresses, on the different diagonals at different locations vary. The strains in those members toward the center of the bridge are higher compared with the ones closer to the abutments.

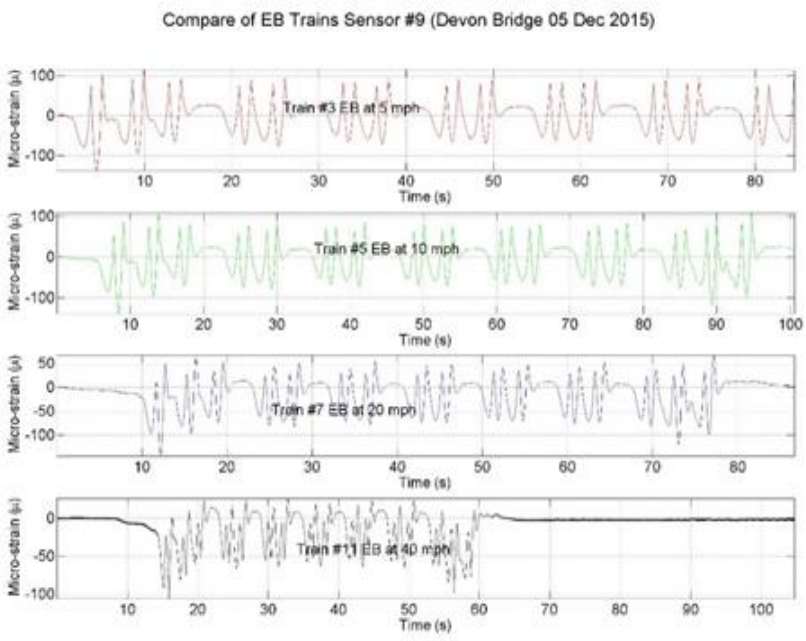

FIGURE 22. Strain from field on running rail at various train speeds.

Figure 24 shows the locations of the strain sensors attached to the different sides of the two eyebars in diagonal M7-L8 in the south truss (see Figure 7a). Figure 25 presents the corresponding strain readings. It can be clearly seen that the strain readings corresponding to the two eyebars, even though they are conneted to the same joints and are different not only in terms of magnitudes but also in the nature of their variation with time as the train moves over the bridge.

Figure 26 shows the strain sensor locations on 4 of 10 eyebars constituting the bottom chord of the south truss between joints/nodes L6 and L8 (see Figure 7). Figure 27 shows corresponding strain data recorded under the westbound Waterbury train travelling at 16 km/h (10 mph). It can be seen that the strains in the eyebars vary from each other, even

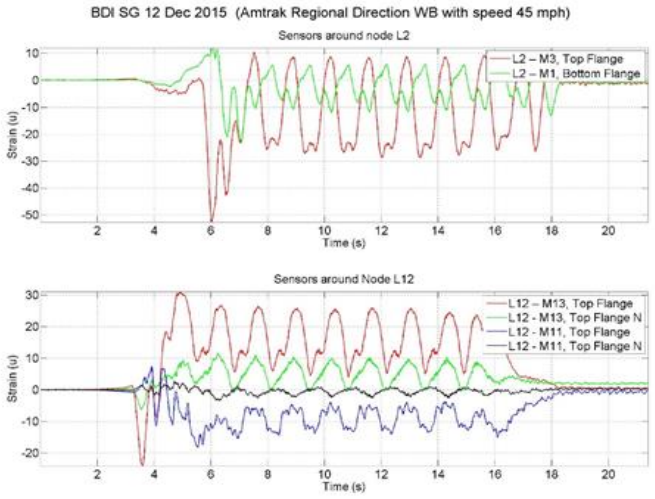

FIGURE 23. Strain from field tests on different diagonals attached to the lower chord nodes, L2 and L12. See Figure. 7(a) for diagonal locations.

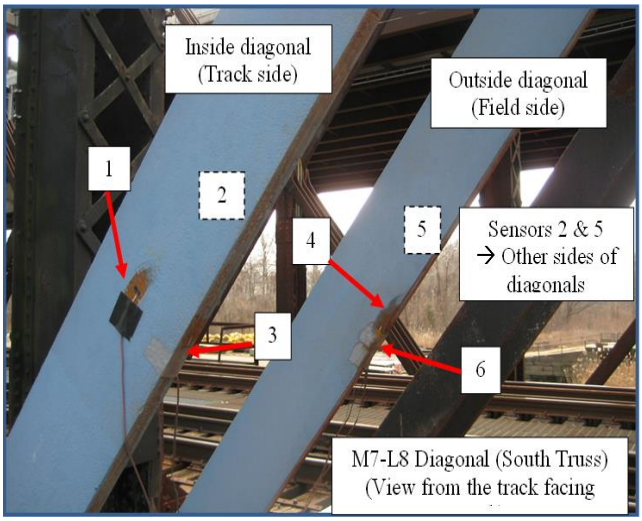

FIGURE 24. Location of strain sensors (strain gage) attached on eyebars of diagonal M7-L8 (south truss).

though they are connected to the same two joints. Especially, the strain in the eyebar corresponding to sensor #23 (attached to the eyebar farthest from the track) is small compared with the others. It could be that due to excessive and uneven wear on the outer edges of eyebar pin holes, strain is not taken evenly by all the eyebars in a group. Rather, the shorter eyebars start to take tension under load. As the shorter eyebar lengthens, the slightly longer eyebars gradually become engaged and then start taking load. This phenomenon may result in temporary overstress (although it might not be beyond yield) in the shorter eyebars and excessive vibration in the longer eyebars. This problem of older eyebar trusses has been also previously observed (BDI 2001; Walls et al. 2002; BDI 2008; Mazurek 2011).

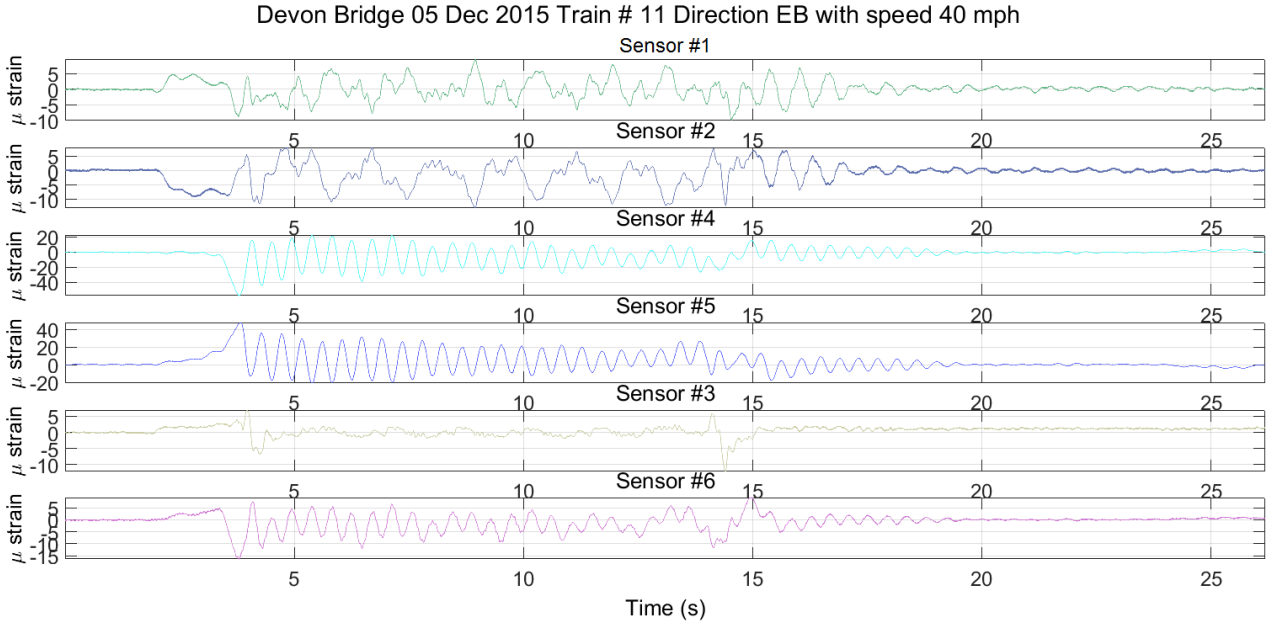

FIGURE 25. Strain readings on different locations of the two eyebars in diagonal M7-L8 (south truss). See Figure 7(a) for diagonal locations and Figure 24 for sensor locations.

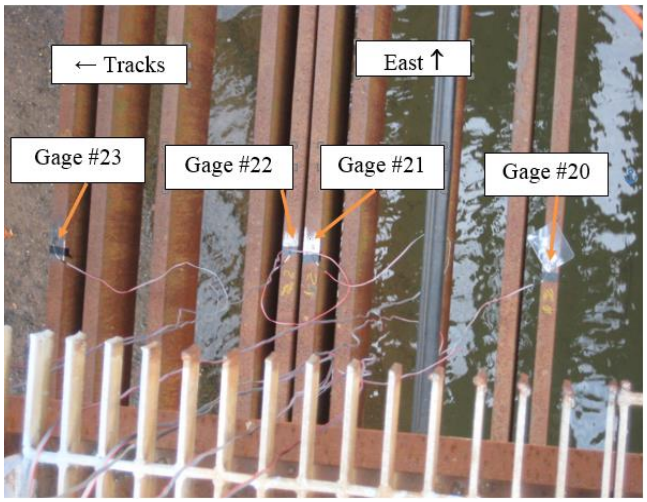

FIGURE 26. Location of foil strain sensors, lower chord L6-L8, south truss (a set of 10 eyebars, each 10" x 1 7/16" in cross section).

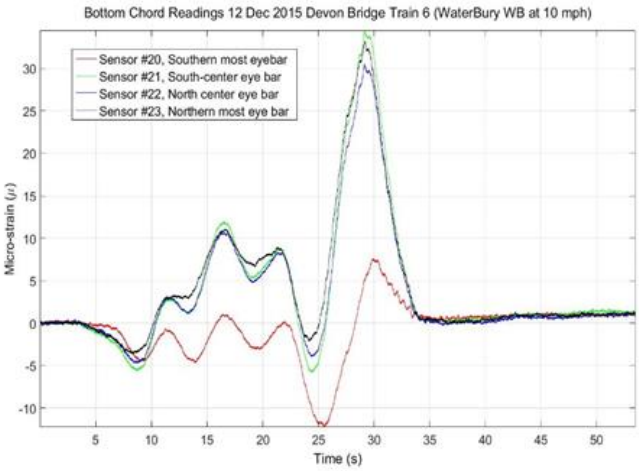

FIGURE 27. Strain readings on different eyebars on bottom chord L6-L8 south truss under Waterbury train westbound on track 3 at 16 km/h (10 mph).

4.7.3 Processing of Field Acceleration Data

Ambient testing of a bridge under moving vehicles helps to obtain the modal parameters of the bridge (Yang et al. 1995). In order to obtain the natural frequencies and mode shapes of bridge vibration, the accelerometer data collected from the field test in the Devon Bridge was processed using MATLAB (Math Works 2014). The acceleration signals obtained from different field tests were separated as forced vibration (when a train was on the bridge) and free vibration (after the train crossed over the span) of the bridge as shown in Figure 28 and processed separately.

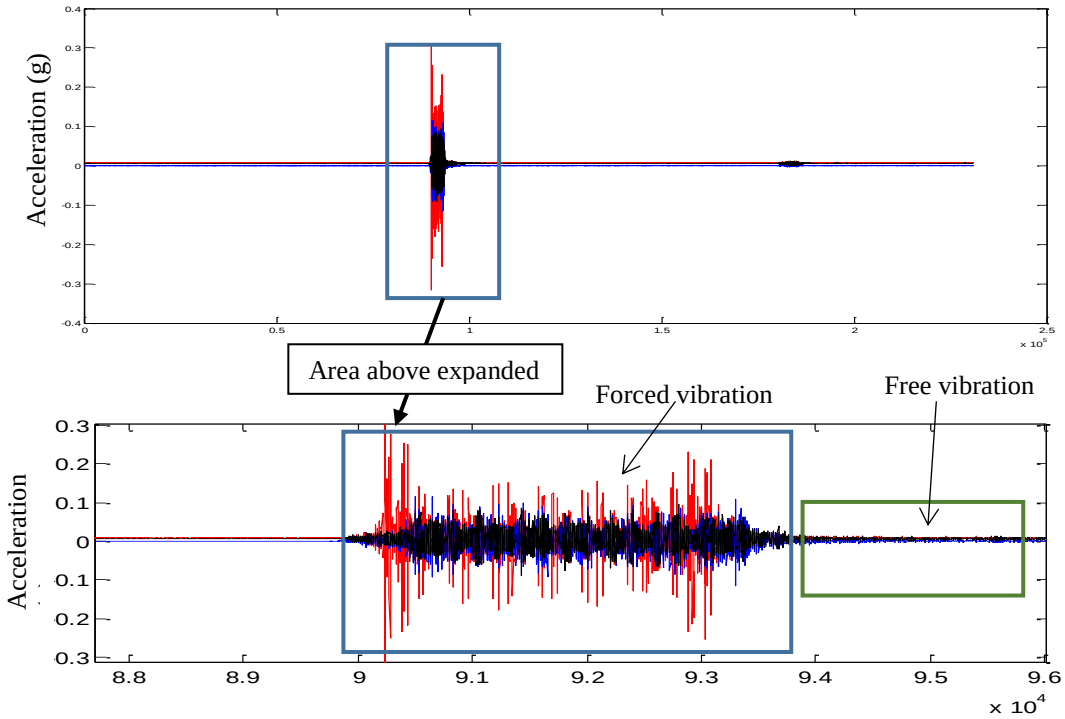

FIGURE 28. Free and forced vibration field test acceleration signal of the bridge span.

4.7.3.1 Power spectral density and singular value decomposition

The power spectral density (PSD) is the frequency response of random or periodical signals. The PSD shows the strength of the energy as a function of frequency. It gives information about the frequencies with high energy in the obtained signal. PSD of an acceleration signal measured using the accelerometers in the field testing of a structure will help to identify the natural frequencies of a structure. The singular value (SV) decomposition (SVD) is a technique of handling a square matrix that does not have an inverse. The SVD will help to reduce noise in a measured signal. The SVD of the PSD matrix, containing the PSD values computed from a set of acceleration data, will help better to identify the natural frequencies, which appear as a distinct peak of a SV matrix.

The raw acceleration data collected from the field test of the Devon Bridge span was first detrended to remove any trends and the PSD values were obtained. Detrending of raw acceleration signal removes the mean value or linear trend from a signal and is often used in signal processing in frequency domain (Math Works 2014). The PSD values were further processed to obtain SV through the SVD technique using the MATLAB code. The sample PSD and SV plots for one case of field setups are shown in Figures 29 and 30. Legends Acc P1, Acc P2, Acc P3, Acc P4, and Acc P5 in the figures refer to the PSD values generated from the acceleration signals of accelerometers placed at locations P1, P2, P3, P4, and P5 on the bridge, respectively.

4.7.3.2 Natural frequencies and mode shapes

From the field acceleration data, the natural frequencies of Devon Bridge span 7 were identified from the most recurring peaks of PSD and/or SVD versus frequency curves. For the free vibration response of the bridge, the first as well as the second natural modes of bridge vibration were in the lateral direction at frequencies 1.758 Hz and 3.34 Hz, respectively (not shown here). The first vertical mode of bridge vibration was identified at frequency 4.668 Hz (Figure 29).

Identification of other higher modes and their natural frequencies was not possible (from ambient vibration of bridge at a particular speed of train) as the peaks of SV versus frequency were inconsistent and had numerous peaks above 5 Hz. The PSD and SV curves were also generated for the forced acceleration response of the bridge. These curves contain the peaks corresponding to natural free vibration frequencies of the bridge, as well several peaks corresponding to various other frequencies. Figure 30 shows the PSD and SV curves for the vertical direction.

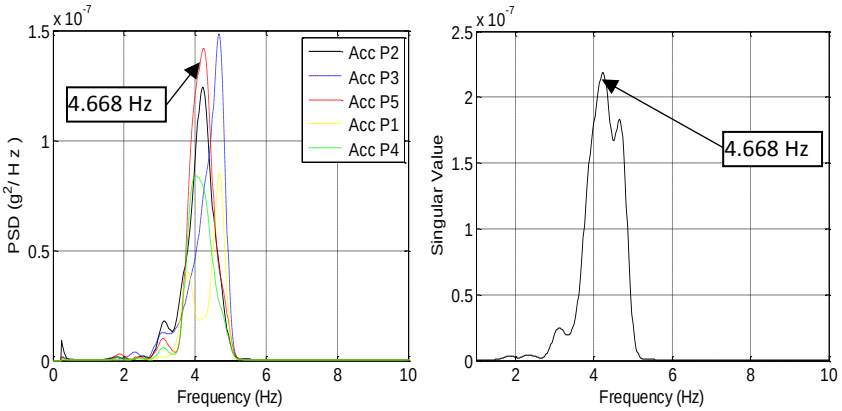

FIGURE 29. PSD and SV for the free vibration response in vertical direction.

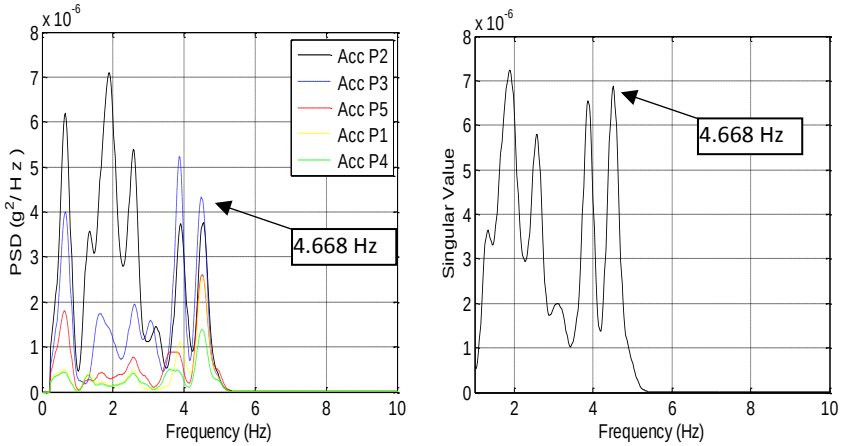

FIGURE 30. PSD and SV for the forced vibration response in vertical direction.

The mode shapes of bridge vibration were also obtained from the processing of the accelerometer field data excited by the moving trains. The PSD values corresponding to natural frequency of vibration for a particular mode were obtained for each location of accelerometers on the bridge. The maximum PSD value was used to normalize other values and they were plotted against the location of the bridge to obtain the mode shapes. The mode shapes obtained by processing field test data are shown in Figures 31 and 32 along with the mode shapes obtained from FE model.

4.8 COMPARISON OF BRIDGE RESPONSE FROM FINITE ELEMENT MODEL AND FIELD TESTS

4.8.1 Natural Frequencies

The comparison of the first three natural frequencies of bridge vibration obtained from field test and FEM is shown in Table 8. It can be observed that except for the first mode of vibration, the other two natural frequencies of the Devon Bridge span obtained from the FE analysis are relatively close to that obtained from the field experiment. Some possible causes for the difference in the frequencies are discussed at the end of this section.

TABLE 8. Comparison of the first three natural frequencies obtained from FEM and the field experiment

Global Modes	Natural Frequency (Hz)			Difference (in %) with Respect to Field Experiment	
	FEM		Field experiment	Simplified top bracing	Detailed top bracing
	Simplified top bracing	Detailed top bracing			
First lateral mode	1.256	1.478	1.758	28.56	15.93
Second lateral mode	3.635	3.558	3.34	8.83	6.53
First vertical mode	4.854	4.843	4.6	5.52	5.28

4.8.2 Mode Shapes

The comparison of mode shapes obtained from the FEM and the field experiment for the first and second lateral modes of vibration is presented in Figures 31 and 32, respectively. It can be seen that they are very similar.

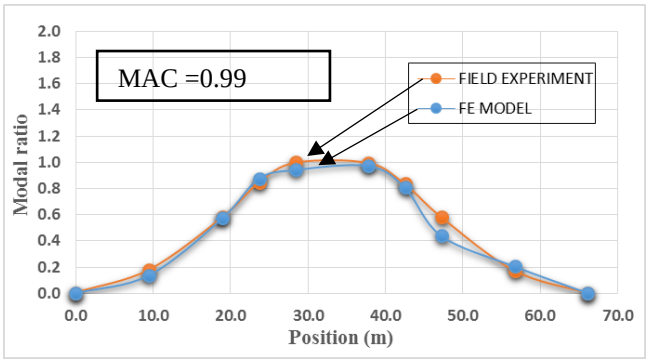

FIGURE 31. Comparison of first lateral mode shapes obtained from FEM and field experiment.

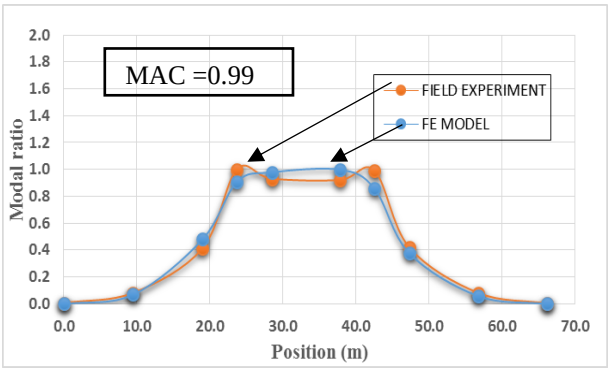

FIGURE 32. Comparison of first vertical mode shape obtained from FEM and field experiment.

4.8.3 Modal Assurance Criterion (MAC)

Modal assurance criterion (MAC) is a technique used to estimate the degree of correlation between mode shape vectors obtained from the field testing and analytical computation (Satoh 1966). The estimation of MAC does not require the estimation of system matrices. The MAC between a measured mode $\emptyset_{mj}$ and an analytical mode $\emptyset_{ak}$ is given as:

$$MAC_{jk} = \frac{\left|\emptyset_{\mathrm{mj}}{}^{T}\emptyset_{\mathrm{ak}}\right|^{2}}{\left(\emptyset_{\mathrm{ak}}{}^{T}\emptyset_{\mathrm{mj}}\right)\left(\emptyset_{\mathrm{mj}}{}^{T}\emptyset_{\mathrm{mj}}\right)} \quad (17)$$

The value of MAC ranges between 0 and 1. MAC value close to 1 shows the strong correlation of the two mode shape vectors. Table 9 presents the mode shape vectors obtained from FEM and the experimental field test for first lateral and first vertical modes of vibration and calculated MAC values for both modes.

The MAC values for both the modes are found to be approximately 0.99 (close to 1), which shows a strong correlation between the mode shape vectors obtained from FEM and the experimental field test of the bridge.

TABLE 9. MAC values for mode shapes obtained from FEM and the experimental field test

Location on Bridge (m)	First Lateral Mode			First Vertical Mode		
	FEM	Field Exp.	MAC	FEM	Field Exp.	MAC
0	0	0	0.994	0	0	0.99
9.48	0.136	0.18		0.07	0.08	
18.96	0.574	0.58		0.48	0.41	
23.7	0.877	0.85		0.91	1	
28.44	0.944	1		0.98	0.93	
37.8	0.975	0.997		1	0.92	
42.53	0.809	0.836		0.859	0.99	
47.26	0.438	0.582		0.38	0.42	
56.71	0.204	0.172		0.06	0.08	
66.16	0	0		0	0	

4.8.4 Vertical Displacement Response with Time

The comparison of the dynamic vertical displacement response of node L7 of the north and south trusses obtained from the FE analysis and the field experiment for an Amtrak Acela train are shown in Figures 33 and 34, respectively. The displacement responses of the Devon Bridge span were obtained for the Amtrak Acela train moving at a speed of 64.4 km/h (40 mph) on track 3 of the bridge toward New York City (westbound). Although there is some slight difference between the magnitudes of displacement response obtained from the FE analysis and field experiment, the nature of the response curves are very similar.

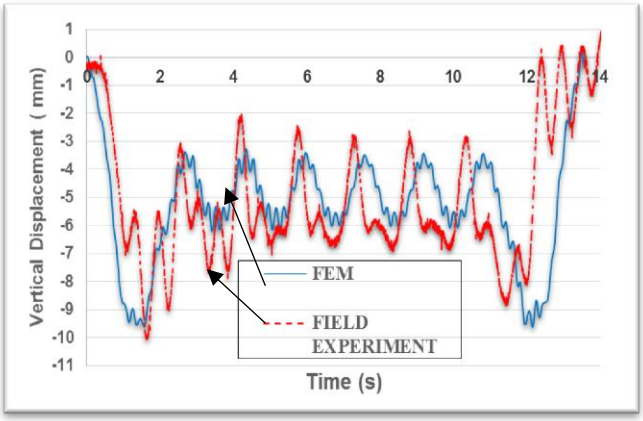

FIGURE 33. Comparison of time history vertical displacement of node L7 of north truss obtained from FEM and field experiment under Amtrak Acela traveling 64.4 km/h (40 mph) on track 3 westbound.

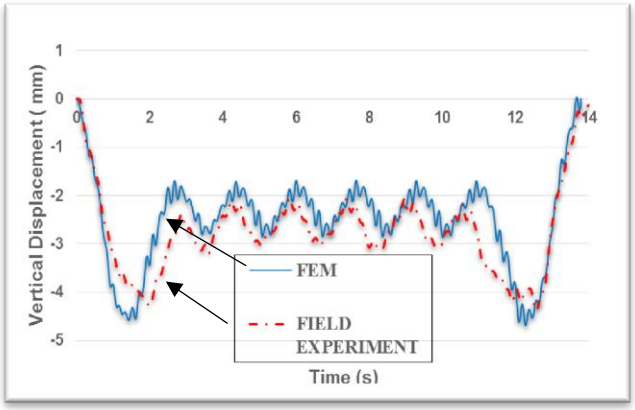

FIGURE 34. Comparison of time history vertical displacement of node L7 of south truss obtained from FEM and field experiment under Amtrak Acela traveling at 64.4 km/h (40 mph) on track 3 westbound.

The discrepancies in natural frequencies and the dynamic displacement response between the values obtained by the FEM analysis and the field tests might be attributed to various inherent and unavoidable differences that exist between the theoretical/computational model and the real structure. Some of these include, but are not limited to, the following: damping/friction caused by the connections between numerous moving parts, the actual effects of the support conditions of the bridge, and the degree of wear in various members (e.g., worn pins and pin holes) all of which are impossible to accurately ascertain by the FEM. Additionally, the rocking effect induced on the bridge structure and the lateral forces on the bridge were not included in the finite element analysis. Furthermore, the vehicle–bridge interaction exists in the actual field condition, whereas that was not exactly reflected in the FEM. These are important subject areas for further study and therefore have been listed under the "Future Research" subsection in the "Conclusions and Summary" section of this report.

4.9 RESONANCE PHENOMENON—RESONANCE TRAIN SPEEDS AND DISPLACEMENTS

The resonant speeds of the trains in vertical and lateral vibrations of the bridge for Amtrak Acela, Amtrak Regional, and Metro–North M8 trains on Devon Bridge as given by Eq. (14) were determined and analyzed using the finite element and analytical relations.

The resonant speeds of Amtrak Acela trains obtained for the first and second lateral modes and first vertical mode of vibration of span 7 of the Devon Bridge are shown in Figure 35. ("Resonance speed" is the speed of the train at which the moving train loading frequency matches with the natural frequency of the bridge.) The i parameter in the abscissa of Figure 35 gives the different index values for the resonant speed. It should be noted that the resonance train speeds computed based on Eq. (14) are considering the truss bridge as an equivalent beam/girder type bridge having the same frequencies.

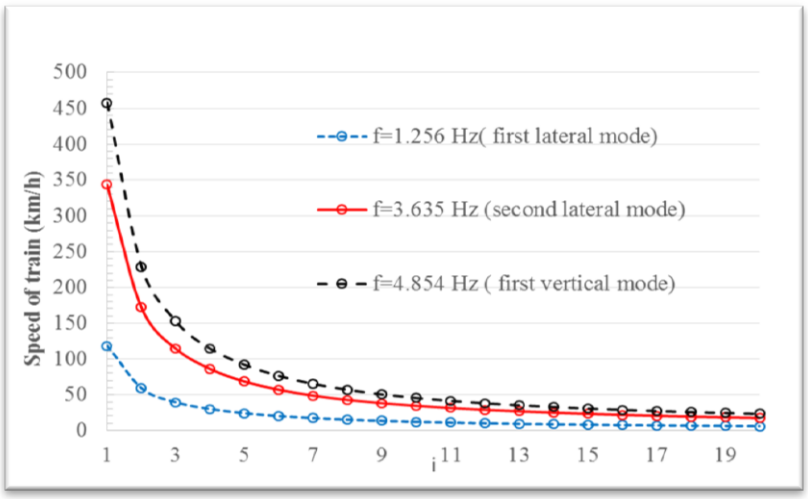

FIGURE 35. Various resonant speeds of Amtrak Acela for the Devon Bridge.

Using the FEM of span 7 of the Devon Bridge, displacement response of a few truss nodes have been determined under the three trains mentioned above moving at various speeds between (2 and 160 km/h (1.2 and 100 mph), and peak displacements were obtained at resonant train speeds given by Eq. (14).

A sample result of the maximum vertical displacements of node L7 on the north truss bottom chord joint under three different train loadings (Amtrak Acela, Amtrak Regional, and Metro–North M8) at various speeds is shown in Figure 36. The peaks seen in the displacement versus speed curve correspond to the resonant speeds computed analytically (Baniya 2015). The results show that as anticipated, the response of the bridge near resonance speeds can increase sharply. Thus, the operations of the train should be avoided near the resonance speeds to prevent the amplification of the response of the bridge and to maintain the safety of the bridge and the passengers in the train.

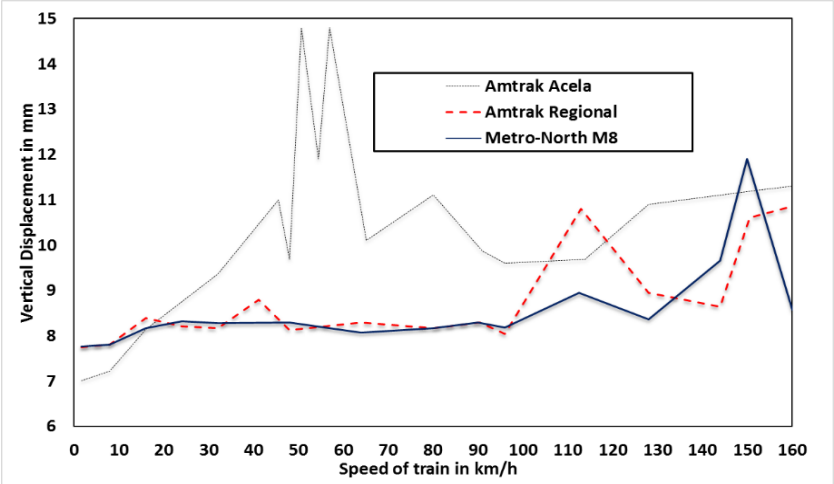

FIGURE 36. Vertical displacement of node L7 of north truss under 3 different train loadings at various speeds.

The comparison of time history (for 5 seconds) of vertical displacement of node L7 of the north truss under a Metro–North M8 train at a resonant speed of 151.5 km/h (94.1 mph) and a non-resonant speed of 64.37 km/h (40.0 mph) is shown in Figure 37. It can be clearly seen that the amplitude of the displacement response of the node considered (L7) is constant as time progresses under the train moving at non-resonant speed. However, the displacement is observed to rise continuously, although in gradual fashion, under the train moving at resonant speed.

From the FE analysis, it was also found that within the speed range considered for the analysis [2 km/h–160 km/h (1.2–100 mph), the first primary resonant condition in lateral direction (which gives highest response) could be excited, but the first primary resonant speed in vertical displacement could not be excited because it was beyond the range of speeds considered.

As can be seen in Figure 36, there is distinct and significant change (mostly increase) in the displacement of the L7 node in 40 km/h (24.86 mph) to 70 km/h (43.50 mph) speed range under Amtrak Acela train loading. However, from the field test results collected at five discrete speed values of 8.0, 16.1, 32.2, 489.3, and 64.4 km/h (5, 10, 20, 30, and 40 mph, respectively), no change in displacement magnitude of this node with speed was observed. This discrepancy might be attributed to various inherent and unavoidable differences between the FEM and the real structure including those described in the last paragraph of the previous section (subsection 4.8.4). Moreover, it should be noted that the resonance train speeds for the truss bridge under consideration were determined using the relationship (Eq. 14) developed for a girder (beam-type) bridge. That means the actual truss bridge was approximated as an equivalent girder/beam. Furthermore, due to the inherent limitation of any sensor and data collection devices, the measurement of response can be accomplished only at discrete points in time. Although during the field testing, the time interval between any two readings was set very small, the reading was not collected exactly continuously. Therefore, it could be possible that the resonance peak displacements were missed from the recording. This is because the resonance effect is more prominent only at or very close to the resonance speed. As the train moves faster or slower than the resonance speed the resonance effect reduces very quickly. These are important subject areas for further research in the future and, therefore, have been listed under Section 6.2 ("Future Research") of this report.

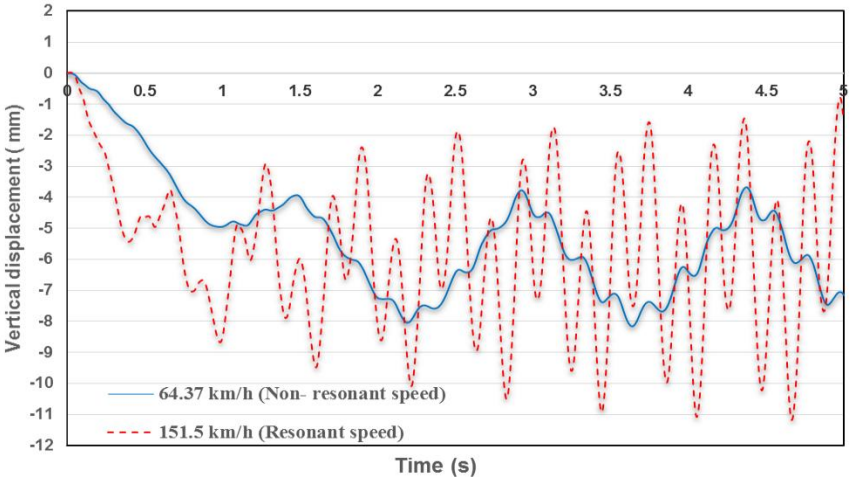

FIGURE 37. Comparison of vertical displacement of node L7 of north truss of Devon Bridge under Metro-North M8 train.

5. PLAN FOR IMPLEMENTAION

The results obtained from this study have so far been disseminated through several presentations and publications at conferences, seminars, reports, thesis, and journals (Malla 2015; Malla et al. 2016a, 2016b, 2016c; Jacobs et al. 2015, 2016; Baniya 2015). Publication and presentations of the research results will continue in the future. The knowledge gained will be shared with and made available to railroad bridge designers and the railroad industry through presentations to AREMA and other venues. So far, three graduate students at M.S. and Ph.D. levels have been trained through this research. Two other graduate students, one at the M.S. level and another at the Ph.D. level, received experience by becoming involved in the field testing phase of this project. One Master's degree thesis has already resulted (Baniya 2015) and at least one Ph.D. dissertation is expected from this study.

The results from this research project can help engineers better understand effects of train speed on railroad bridge structures; hence, impact factor determination. This in turn should contribute to more efficient, durable, and economic designs of new bridges, and more accurate ratings of existing bridges. Therefore, the results from this study will be highly relevant to the federal and state departments of transportation, industries dealing with railroad bridge design, construction and maintenance, and railroad transportation service providers. Several railroad companies, as well as Committee 15 (Steel Structures) of AREMA, have already expressed interest in the results and conclusions of this research effort.

As a part of the implementation, it is also recommended that future research studies in certain key areas associated with this research study as listed below in Subsection 6.2 ("Future Research") under Section 6 ("Summary, Conclusions, and Future Work") be carried out.

6. SUMMARY, CONCLUSIONS, AND FUTURE WORK

The dynamic response of a railroad bridge structure subjected to moving vehicles (trains) is a complex interaction between these two systems. The factors affecting the response for railroad bridges are many as listed under the Impact Factor Concept subsection of this report. Despite more than 100 years of research on dynamic amplifications and impact factors of railroad bridges, results have often been conflicting and inconsistent. This has led to frequent modifications of the design impact formulas for railroad bridges over time. With the constant improvement in the technology of sensors, as well as the use of modern computers for improving analytic and computational methods, it is reasonable to assume that the formulas used today, as well as future refinements of the formulas, are and will be more accurate mathematical expressions of the actual physical response of the railroad bridge structures.

6.1 SUMMARY AND CONCLUSIONS

The stated objectives of the project were fully achieved with work performed in two stages, Stages 1 and 2. The main focus in Stage 1 included the development of the finite element model (FEM) and analysis of the test bridge with initial field testing and comparison of the results. The activities in Stage 2 consisted of further detail field testing of the bridge with trains traveling at varying speeds, comparison of results and refinement of the FEM, and investigation on resonance speed of the trains for the bridge. Several delays were encountered during the field test portion of the project, resulting in this phase of the work taking longer to complete than planned. Delays resulted from bad weather and the un-availability of test train equipment and crews. Owing to this, the project received two, 6-month long, no-cost extensions for completion.

In this research, a thorough and comprehensive literature search and review of related research articles, papers, and reports were performed. A comprehensive FEM of the long span through-truss Devon railroad bridge over Housatonic River, Milford, Connecticut, was developed and static (including train live load) modal and dynamic/time history analyses were performed to obtain bridge response (displacements and stresses), frequencies, and mode shapes.

A series of field tests were conducted on the Devon Bridge over a period of 16 months and significant amounts of data relating to the structure's response, including accelerations, displacements, and strains were collected using accelerometers, linear variable differential/displacement transducers (LVDTs), and strain gages. The bridge response parameters were measured while the bridge was subjected to various types of trains, including Amtrak Acela, Amtrak Regional, Metro–North commuters cars, and Waterbury Branch trains traveling at or near 64.4 km/h (40 mph, the current speed limit on the bridge) and at slower speeds of 8.0, 16.1, 32.2, and 48.3 km/h (5, 10, 20, and 30 mph, respectively). The field test data were analyzed to extract frequencies, mode shapes, and displacements of the bridge. The bridge response parameters obtained from field tests and FEM analyses have been compared and correlated to update the FEM.

Further finite element analysis to obtain the railroad bridge response incorporating higher train speeds was however not possible due to the FE software limitation that restricted modeling of dynamic train loads up to a maximum of 160 km/h (100 mph). Similarly, field tests could not be conducted at train speeds higher than 64.37 km/h (40 mph) because of the strict speed limit on the Devon Bridge imposed by the Metro–North Railroad Company, which is responsible for operating the railroad line.

In summary, a few of the conclusions that can be drawn/inferred from this research study include the following:

- A highly accurate and reliable FEM of a complex bridge structure, when the model is continuously updated and refined as field data becomes available, provides an extremely useful and robust tool for projecting impact and other bridge responses (displacement, strains, vibration modes) from trains at speeds higher than those currently operating on the bridge. This ability to forecast, or predict, is valuable in assessing bridge safety and future performance, which is especially important in older bridges.
- A strong correlation of the field test results with those values obtained from the FEM has given relatively good confidence in using the FEM as a predictive tool for the bridge response under a train moving at speeds higher than the current allowable operating speed of 64.37 km/h (40 mph).
- The resonant speeds in vertical and lateral direction for Amtrak Acela, Amtrak Regional, and Metro–North M8 trains on the Devon Bridge span were determined and identified for the speed range of 2 km/h–160 km/h (1.2–100 mph) using the finite element and analytical relations. It was found that within this speed range, first primary resonant condition (which gives highest response) in the lateral direction, could be excited, but the first

primary resonant speed in vertical displacement could not be excited as it was beyond the range of speeds considered.

- Results from the finite element analysis of the bridge also indicated that at resonant speeds [speeds of the train at which the frequency of the loading (excitation) under which the bridge is subjected to matches with the natural frequency of the bridge], there is a sudden rise in the displacement of a point on the bridge, and different trains would induce this peak displacement at different speeds. This indicates a clear relationship between vehicle speed and bridge response; hence, the impact factor, although the exact speed is a function of the train's axle spacings and loads. However, the results obtained from the field tests with train speeds of 8.0, 16.1, 32.2, 48.3, and 64.4 km/h (5, 10, 20, 30, and 40 mph) did not match with the analytical (finite element) assessment regarding the dynamic amplification of the bridge response near resonant speeds. This discrepancy can be attributed to various factors, including the inherent differences that exist in any analytical/finite element modeling and actual real-life field conditions.
- Strain gage data from eyebars making up the truss's bottom chord and diagonal counters show evidence of a problem common to many old truss bridges; that is, excessive and uneven wear at the eyebar holes and pins result in the total tension load not being assumed equally and simultaneously by all eyebars in a group making up the bottom chord. This phenomenon could result in the shorter eyebars temporarily experiencing stresses greater than what they were designed for, while the longer eyebars may experience excessive vibrations when trains are on the bridge.

6.2 FUTURE RESEARCH

Although this study has highlighted the effects of speed on the dynamic impact factors on the bridge, further investigation will be needed to determine the actual relationship between speed and impact factor that can be used for design and rating purposes. To achieve this, additional research related to the work described in this report is recommended in areas described below (but not listed in any priority order):

1. Develop actual relationship between vehicle speed and impact factor for a railroad bridge;
2. Investigate the effects of the lateral load generated by the moving trains on the bridge structure;
3. Investigate the couple effect of impact (stiffness) and resonance (deflection) as related to the live load impact factors;
4. Study the relationship between high speed rail passengers' riding comfort as a function of interaction between the vehicle suspension and bridge structure;
5. Study the effect of interaction between the moving vehicle dynamic properties (e.g., mass, moments of inertia, damping, stiffness of suspension systems, etc.) and the bridge dynamic characteristics on the structural response of the bridge;
6. Investigate the rocking effect on a truss bridge from trains at higher speeds;
7. Develop methodology and relations to determine resonance and cancellation speeds of a moving train specialized for truss railroad bridges;
8. Develop methodology to determine optimum sensor numbers and locations on a truss railroad bridge for efficient and effective field testing;
9. Develop efficient and accurate methodology to extract bridge dynamic response (displacements and stresses) and features (frequencies and mode shapes) from data collected using a limited number of sensors (i.e., limited field test data) for truss-type railroad bridges; and
10. Conduct field tests of railroad bridges at train speeds higher than 64.4 km/h (40 mph), the prescribed maximum speed limit at the bridge in this study, to more fully understand the speed effects on the bridge response.

Several tangible positive outcomes should result from this study. A clearer understanding of impact as it relates to vehicle speed and bridge resonance could be used to more accurately approximate stress range, which is a major component of fatigue analysis. Stress range, coupled with the number of stress cycles, if known more accurately, could result in an extended life cycle for existing bridges. This in turn directly translates into increased bridge safety, as well as future costs, as it extends the time at which bridge replacement becomes necessary. Another equally important benefit would be reducing costs of possible upgrades of older bridges to accommodate higher speed trains. This would be possible with better understanding and knowledge of bridge response from impact at higher train speeds.

7. REFERENCES

Amtrak, "Priority of Northeast for High Speed Rail," Amtrak (National Passenger Rail Corporation), Washington, D.C., 2016 [Online]. Available: http://www.nec.amtrak.com (accessed July 11, 2016).

AREA Committee 30, "Test Results on Relation of Impact to Speed," *Proceedings*, American Railway Engineering Association (AREA), Vol. 50, AREA, Chicago, Ill., 1949, pp. 432–443.

AREA Committee 30, "Report of Committee—Impact and Steel Stresses," *AREA Bulletin 611*, American Railway Engineering Association (AREA), Chicago, Ill., 1968, pp. 450–451.

AREMA, "Historical Sketch of the Development of American Bridge Specifications," *Proceedings of the 6th Annual Convention*, American Railway Engineering and Maintenance of Way Association, Vol. 6, AREMA, Chicago, Ill., 1905, pp. 199–217.

AREMA, "Committee XV Impact Tests on Railway Bridges," *Bulletin No. 125*, American Railway Engineering and Maintenance of Way Association (AREMA), 1910, Chicago, Ill.

AREMA—Committee 30, "Report of Subcommittee Work on Bridge Impact," *Proceedings*, American Railway Engineering and Maintenance of Way Association (AREMA), Lanham, Md., Vol. 12, Part III, 1911, pp. 15–56.

AREMA, *Manual for Railway Engineering*, American Railway Engineering and Maintenance of Way Association (AREMA), Lanham, Md., 2016.

Association of American Railroads (AAR), *Field Investigation of a Truss Span on the Great Northern Railway*, Report No. ER-81, AAR Research Center, Chicago, Ill., 1968a.

Association of American Railroads (AAR), *Field Investigation of Two Truss Spans on the Southern Pacific Company*, Report No. ER-82, Association of American. Railroads (AAR) Research Center, Chicago, Ill., 1968b.

Baniya, S., "Modeling and Analysis of a Steel Truss Railroad Bridge Traversed by Trains at Various Speeds," M.S. Thesis, Department of Civil & Environmental Engineering, University of Connecticut, Storrs, 2015.

BDI, *Load Test and Rating Report, Puget Sound & Pacific Railroad Bridge, Steel Through-Truss Bridge—MP 1.7, Centralia, WA*, Final Report, Bridge Diagnostics, Inc. (BDI), Boulder, Colo., 2001.

BDI, Structural Testing of Bridge No. 08080R, Metro–North Railroad Over Housatonic River, Stratford, Connecticut, Final Report, Bridge Diagnostics, Inc. (BDI), Boulder. Colo., 2008.

BDI, *BDI Strain Gage Model No. ST 350 Operations Manual*, Rev. 2, Bridge Diagnostics, Inc. (BDI), Boulder, Colo., 2012 [Online]. Available: http://bridgetest.com/wp-content/uploads/ST350-Operations-Manual-v2.2.pdf (accessed Oct. 05, 2014).

BDI, *Accelerometer Operations Manual*, Rev. 1.2, Bridge Diagnostics, Inc. (BDI), Boulder, Colo., 2013 [Online]. Available: http://bridgetest.com/wp-content/uploads/Accel-Operations-Manual-v1.2.pdf (accessed Oct. 5, 2014).

Bentley, *STAAD.Pro V8i* (*SELECT series 6*) *Technical Reference Manual*, Bentley Systems, Exton, Pa., 2012.

Biggs, J.M., *Introduction to Structural Dynamics*, McGraw-Hill, Inc., New York, N.Y., 1964, pp. 315–325.

Chu, K.H., V.K. Garg, and C.L. Dhar, "Railway-Bridge Impact: Simplified Train and Bridge Model," *Journal of the Structural Division*, Vol. 105, No. 9, 1979, pp. 1823–1844.

Clough, R.W. and J. Penzien, *Dynamics of Structures*, 3rd ed., Computers and Structures, Inc., Calif., 1995.

Conway, W.B., "Practical Application of the Rating Rules," *Proceedings*, 2001 American Railway Engineering and Maintenance-of-Way Association Conference, AREMA, Landover, Md., Sept. 1–9, 2001 [Online]. Available: http://citeseerx.ist.psu.edu/viewdoc/download;jsessionid=CBF527841D5A5E424B0105FFB049262F?doi=10.1.1.524.789&rep=rep1&type=pdf (accessed Feb. 26, 2017).

Dhar, C.L., K.H. Chu, and V.K. Garg, "Dynamic Response of a Single Railway Truss Bridge," *TRR No.665, Bridge Engineering*, Vol. 2, Transportation Research Board, National Research Council, Washington, D.C., 1978, pp. 73–80.

Frýba, L., "A Rough Assessment of Railway Bridges for High Speed Trains," *Engineering Structures*, Vol. 23, No. 5, 2001, pp. 548–556.

Fryba, L., *Vibration of Solids and Structure under Moving Loads*, 3rd ed., Thomas Telford Publishing, London, U.K., 2013.

Goicolea, J.M. and F. Gabaldon, "Design Issues Related to Dynamics Effects for High-Speed Railway Bridges in Spain," *Dynamics of High-Speed Railway Bridge: Selected and Revised Papers from the Advanced Course on 'Dynamics of High-Speed Railway Bridges,'* Routledge Publishing, New York, N.Y., 2008, pp. 13–24.

Goicolea, J.M., F. Gabaldon, and F. Riquelme, "Design Issues for Dynamics of High Speed Railway Bridges," *Dynamics of High-Speed Railway Bridges: Selected and Revised Papers from the Advanced Course on Dynamics of High-Speed Railway Bridges*, Routledge Publishing, New York, N.Y., 2008, pp. 1–8.

Gu, G., A. Kapoor, and D.M. Lilly, "Calculation of Dynamic Impact Loads for Railway Bridges Using a Direct Integration Method," *Journal of Rail & Rapid Transit—Proceedings of the Institute of Mechanical Engineering, Part F*, Vol. 222, 2008, pp. 385–398.

Hamidi, S.A. and F. Danshjoo, "Determination of Impact Factor for Steel Railway Bridges Considering Simultaneous Effects of Vehicle Speed and Axle Distance to Span Length Ratio," *Engineering Structures*, Vol. 32, No. 5, 2010, pp. 1369–1376.

Hunley, J.B., "Impact in Steel Railway Bridges of Simple Span," *Proceedings*, American Railway Engineering Association (AREA), Vol. 37, AREMA, Chicago, Ill., 1935, pp. 740–939.

Jacobs, D.W., S. Dhakal, S. Baniya, and R.B. Malla, "Investigation of an Old Open Deck Truss Railroad Bridge: Field Testing and Finite Element Models," ASCE SEI 2015 Structures Congress, Portland, Ore., April 2015.

Jacobs, D.W., S. Dhakal, R.B. Malla, and Z.Y. Wu, "Need for Development of Robust Software Tool for Steel Railroad Bridge Rating," *Proceedings, 8th International Conference on Bridge Maintenance, Safety and Management*, CRC Press, Boca Raton, Fla., June 2016, pp. 1438–1442 .

Lu, Y., L. Mao, and P. Woodward, "Frequency Characteristics of Railway Bridge Response to Moving Trains with Consideration of Train Mass," *Engineering Structures*, Vol. 42, Sept. 9–22, 2012.

Malla, R.B., "Impact of High Speed Trains on Old Railroad Bridges," *Year in Infrastructure* (*YII*) *Conference*, London, U.K., Nov. 3–5, 2015 (invited presentation).

Malla, R.B., S. Baniya, S. Dhakal, and D.W. Jacobs, "Study of a Long Span Truss Bridge Using the Finite Element Model and Field Experimental Testing," 2016 ASCE–Engineering Mechanics Institute (EMI) Conference, Vanderbilt University, Nashville, Tenn., May 2016a.

Malla, R.B., S. Dhakal, and D.W. Jacobs, "Field Testing and Modeling of Dynamic Response of a Truss Railroad Bridge under Various Train Loads," *Proceedings/Book of Abstracts*, ASCE Engineering Mechanics Institute (EMI) International Conference, Metz, France, Oct. 2016b (invited symposium keynote lecture).

Malla, R.B., S. Baniya, and D.W. Jacobs, "Study of Dynamic and Static Response of an Old Truss Railroad Bridge," *Proceedings*, Earth & Space 2016: ASCE ASD 15th Biennial International Conference on Engineering, Science, Construction, and Operation in Challenging Environments, R.Malla, J. Agui, and P. van Susante, Eds., ASCE, Reston, Va., 2016c, pp. 1052–1062.

Math Works, *MATLAB version 8.3*, Math Works Inc., Natick, Mass., 2014.

Mazurek, D.F., "Effects of End Restraint on Eyebar Behavior in Bridges," *Proceedings*, Society for Experimental Mechanics Conference Series 9999, Experimental and Applied Mechanics, Vol. 6, SEM, Bethel, Conn., 2011, pp. 301–308.

McKeel, W.T. and A.B. Miller, *History of Early Bridge Specifications: A Reprint of a Paper by J. N. Clary*, Report, Virginia Transportation Research Council, Charlottesville, Va., 2006.

McLean, D.I. and M.L. Marsh, *NCHRP Synthesis 266: Dynamic Impact Factors for Bridges*, Transportation Research Board, National Research Council, Washington, D.C., 1998.

NAR, *Bridges to Be Used for High Speed Rail*, The Northeast Alliance for Rail (NAR), New York, N.Y., 2016 [Online]. Available: http://www.northeastallianceforrail.org/2011/08/a-21st-century-nec-the-top-four-failing-bridges-on-the-nec.html (accessed July 12, 2016).

Omega, "OMB-DAQ-3000 Series USB Data Acquisition," OMEGA Engineer, Inc. Stamford, Conn., 2016 [Online]. Available: http://www.omega.com/pptst/KFH.html (accessed Nov. 30, 2016).

Pietraszek, T.T. and G. Oommen, "Static and Dynamic Behaviours of an 85-Year Old Steel Railway Bridge," *Canadian Journal of Civil Engineering*, Vol. 18, No. 2, 1991, pp. 201–213.

Prasad, P., "Engineering Assessment of Steel Railway Bridges Based on Past Performance." *Procs., 2009 Astroads Bridge Conference*, Convention Management Services, Inc., Auckland, New Zealand, 2009, pp. 1–15 [Online]. Available: http://www.cmnzl.co.nz/assets/sm/3579/61/0063-E128Prasad.pdf (accessed May 15, 2016).

Przemyslaw, K., J. Szelazek, K. Sekula, A. Swiercz, K. Mizerski, and P. Gutkiewicz, "Structural Health Monitoring of a Railway Bridge Using Vibration-based and Ultrasonic Methods," *Smart Materials and Structures*, Vol. 20, No. 3, 2011, pp. 1–10.

Rodrigues, J., "Dynamic Performance of a Steel Truss Bridge Under Railway Traffic" *Proceedings, Conference on Structural Dynamics-No.20, SPIE Proceedings*, Vol. 4753, No. 2, Society of Photo-Optical Instrumentation Engineers (SPIE), Bellingham, Wash.

Ruble, E.J., "Impact in Railroad Bridges," *Proceedings of the American Society of Civil Engineers*, New York, N.Y., Vol. 81, No. 736, 1955, pp. 1–36.

Satoh, Y., "Railway Track Structure for High-speed Train," *Quarterly Reports*, Vol. 7, No. 1, Railway Technical Research Institute, Tokyo, Japan, 1966, pp. 39–41.

Timoshenko, S.P., *History of the Strength of Materials*, McGraw-Hill, New York, N.Y., 1953.

TransTeK, "TransTek Series 240 General Purpose DC LVDTs," TRANS-TEK, Inc., Ellington, Conn., 2016 [Online]. Available: http://transtekinc.com/products/series-350/ (accessed Jan. 2015, 2016).

Trimble, "Trimble 147a-01/3 High Resolution Accelerometer," Trimble Navigation Limited, Sunnyvale, Calif., 2015 [Online]. Available: http://www.trimble.com/ (accessed Oct. 18, 2015).

Unsworth, J.F., *Design of Modern Steel Railway Bridges*, CRC Press, Boca Raton, Fla., 2010.
Uppal, A.S., D.E. Otter, and B.E. Doe, *Impact Loads in Railroad Short Steel Bridge Spans*, Report R-964, Association of American. Railroads (AAR), Transportation Technology Center, Inc., Pueblo, Colo., iii, 1, 2003, pp. 18–19, A4–A5.
Walls, D., Jr., J. Porter, and R. Brooks, "Eyebar Maintenance on Steel Bridges," *Proceedings*, Annual Conference of American Railway Engineering and Maintenance-of Way Association (AREMA), Landover, Md., 2002, pp. 1048–1060.
Xia, H., N. Zhang, and W.W. Guo, "Analysis of Resonance Mechanism and Conditions of Train–bridge System," *Journal of Sound and Vibration*, Vol. 297, No. 3–5, 2006, pp. 810–822.
Yang, Y., S. Liao, and B. Lin, "Impact Formulas for Vehicles Moving over Simple and Continuous Beams," *Journal of Structural Engineer*, Vol. 121, No. 11, 1995, pp. 1644–1650.
Yang, Y.B., J.D. Yau, and Y.S. Hsu, "Vibration of Simple Beams Due to Trains Moving at High Speeds," *Engineering Structures*, Vol. 19, No. 11, 1997, pp. 936–944.
Yang, Y.B., J.D. Yau, and Y.S. Wu, *Vehicle–Bridge Interaction Dynamics: With Applications to High-Speed Railways*, World Scientific Publishing, Hackensack, N.J., 2004.
Yoon, H., W.J. Chin, J. Kwark, and E.S. Hwang, "Computation of Impact Factor of High-Speed Railway Bridge by KTX Train Riding Test," *Engineering*, 2013, pp. 751–755.
Zhai, W.M., Q.C. Wang, Z.W. Lu, and X.S. Wu, "Dynamic Effects of Vehicles on Tracks in the Case of Raising Train Speeds," *Proceedins of the Institution of Mechanical Engineers, Part F: Journal of Rail and Rapid Transit*, Vol. 215, No. 2, Mar. 2001, pp. 126–135.